UNIVERSITY OF GHANA, LEGON

HYDROTHERMAL ALTERATION INTERPRETATION OF LANDSAT AND ASTER DATA FOR IRON ORE DETECTION IN THE SHEINI AREA, NORTH EASTERN GHANA.

BY

DELALI DAGODZO

(10440156)

THIS THESIS IS SUBMITTED TO THE UNIVERSITY OF GHANA, LEGON IN PARTIAL FULFILLMENT OF THE REQUIREMENT FOR THE AWARD OF MSC MINERAL EXPLORATION

OCTOBER, 2014

DECLARATION

This dissertation is the result of a research work undertaken by Delali Dagodzo in the Department of Earth Sciences, University of Ghana, under the supervision of Dr. Thomas Armah and Prof. Prosper M. Nude.

…… ..……

DELALI DAGODZO DATE

(Student)

…… ……..…..

DR. THOMAS ARMAH DATE

(Principal Supervisor)

…… ……..

PROF. PROSPER M. NUDE DATE

(Co-Supervisor)

ABSTRACT

The Sheini Hills in the Zabzugu/Tatale area of the Northern Ghana has one of the finest iron ores in Africa. The surface of the bare area at Sheini Hills is large and vegetation is few, so the extraction of mineral anomaly alteration from LANDSAT Enhanced Thematic Mapper (ETM) and Advanced Spaceborne Thermal Emission and Reflection Radiometer (ASTER) data is feasible, yet most mineral exploration concepts have failed to recognize the association of mineralization with alteration zones using remote sensed data. The area is an excellent environment to experiment with remote sensing for identifying iron ore. The ore deposits have iron-rich caps or gossans with distinct reflectance spectra. The large size of the gossans and associated alteration zones will make them easily detectable with orbital remote sensing platforms, such as Landsat ETM and ASTER.

The purpose of this project is to develop the procedures and demonstrate the feasibility of using multispectral remote sensed data to identify alteration zones associated with iron ore deposition in the study area. The multispectral remotely sensing datasets that have been used in this research are comprised of the LANDSAT Enhanced Thematic Mapping (ETM+) and the Advanced Space borne Thermal Emission and Reflection Radiometer (ASTER). In this work, several advanced image processing techniques such as color composites, band ratios, principal components analysis (PCA) and the crosta technique was applied and tested. These images were produced to highlight important areas of hydrothermal alteration associated with iron ore deposition. Iron-oxide anomaly alteration was extracted by PC 3 on TM band1, band3, band4 and band7.

The results indicated good correlation between locations of hydrothermal alteration zones observed from the satellite images with the mapped iron formations, ferricretes and mapped quartzites. In this way LANDSAT and ASTER has been proven to be a powerful tool in the initial steps of ore deposit exploration.

The images produced proved to be useful in identification, detection, and delineation of hydrothermal alterations, and lithological rock units associated with iron ore deposits in the research area of the Sheini Hills. The ASTER data was processed for alteration assemblages associated with banded iron formation deposits. The Landsat ETM+ data was processed for iron oxides and generalized clay alteration. There is a close correlation between chlorite anomalies and drainage indicating that much of the alteration is related to alluvium along river or stream valleys. Many of the larger carbonate anomalies also coincide with broad areas of alluvium. There is a better correspondence between the Landsat derived haematite/jarosite anomalies and mapped iron formations/ ferricretes.

In the present study, there were no ground data, and the validation was performed on a geological map. The results of this study are based on remote sensing interpretations. As a follow up it would be advantageous to undertake a field based structural analysis to verify/revise and further develop the structural models. Field analysis should be undertaken to verify the geometry and kinematics of the major structures identified from the satellite image interpretations

DEDICATION

This dissertation is dedicated to Almighty God, my mother, Mrs. Sarah Dagodzo and my father, Mr. Kounah Dagodzo.

ACKNOWLEDGEMENT

I thank God very much for everything. I thank my lovely supervisors, Dr, Thomas Armah and Prof. Prosper M Nude who were there for me throughout the troubles I have given them. God richly bless them. A big thank you goes to all the teaching and non-teaching staff of the Department of Geology, University of Ghana, Legon and Cadero Resources Ltd for their help.

Table of Contents

LIST OF FIGURES

LIST OF TABLES

CHAPTER ONE

1.0 INTRODUCTION

1.1 General

Recognition of major mineral deposits formed in association with alteration zones in Ghana has been established and similar occurrences are being recognized globally. In most cases, current mineral exploration concepts have failed to recognize the association of mineralization with alteration zones using remote sensing techniques. Imaging spectroscopy is a new mapping technique and represents a part of the next generation in remote sensing technology. The extraction of metallic minerals (e.g. hematite, limonite, goethite and magnetite) derived from iron ores is important for the product industries utilizing iron and steel and for the infrastructure requirements of agriculture, where the ores can be used as fertilizers. In remote sensing, satellite and airborne multispectral or hyperspectral sensors are used to measure the properties of the land, sea and atmosphere. Compared to the most traditional methods, this technique offers the possibility of covering large areas quickly and often at a relatively low cost. This method is generally used to monitor the state of the environment, to observe and study earth surface processes and to map lithologies and natural resources, such as iron ore deposits. (Salem et al, 2011).

The Sheini Hills Iron Project is a large-scale project located in northeastern Ghana approximately 400 kilometers north of Ghana's capital city, Accra. The Sheini Hills Iron Deposit contains a total Inferred Mineral Resource of 1.312 billion tons grading 33.8% iron. The Hills predominantly comprises bladed hematite with lesser iron hydroxides (goethite, limonite). The source materials in the area appear to be weathered and characterized by a simple colour change

and/or it may involve major textural, mineralogical and/or chemical changes. (Henderson K.J, 2012)

The goals for producing alteration images for this project is to optimally depict all spectral properties that may be related to iron alteration and then prioritize such targets. The presence of hydrothermal mineralization can be a point of start for a mining exploration project, quite often, this type of mineralization can be indicative of a possible deposit of minerals that can be extracted and eventually commercialized with an economical benefit. The remote sensing techniques applied to airborne or spatial data are very useful for a first stage of a regional exploration campaign due to the relatively simple way of covering great surface and obtaining specific emplacements for a more specific study with other on site techniques such as soil geochemistry. Remote sensing instruments can discriminate different spectral characteristics of this type of mineralization, thereby allowing for the detection of different types of surface materials, for example, from Landsat Enhanced Thematic Mapper and ASTER datasets. In the past, geological maps are prepared from conventional ground surveys based on field observations. They are made along traverse lines at regular intervals. While plotting such point information collected along the traverse lines on the topographic base and ultimately preparing final maps by extrapolating the details, certain errors are unavoidable and lead to inaccuracies in maps. Since the development of remote sensing technology, mapping procedures have undergone continuous change. Remote sensing techniques play an important role in mapping programs (Farina et al., 2005). Mapping of lithology and alteration zones in inaccessible mountainous and forested terraines has always posed a challenge. There always existed disputes on the accuracy of lithological boundaries and structural details in these maps. Vast area to be

surveyed and its inaccessibility, forbids physical investigation of every outcrop. At this juncture, the potential of remote sensing is appreciable. The greatest advantage of remote sensing is the synoptic view that it provides. It gives a regional and integrated perspective of inter-relations between various land features. (Drury, 1987)

1.2 Problem Definition

The study area and its environment have been surveyed and studied by several geoscientists, particularly for the subsurface geological mapping and geochemical studies. (Jacques, E. H., 1958). Irrespective of this, only a little attempt has been made so far to understand the detailed relationship between alteration zones observed on the ground and those in remotely sensed images at the study area. The extent of the alteration may be measured in millimeters or kilometers. In most cases, mineral exploration techniques applied in the study area have failed to recognize the association of mineralization with alteration zones, yet some alteration assemblages are of sufficient scale and predictability that they can be used to increase the target size when exploring for new ore deposits.

In view of the above it is anticipated that the enhancement and interpretation of multispectral remote sensing data such as LANDSAT and ASTER may be useful in the detection, and delineation of lithological rock units and hydrothermal alterations associated with iron ore deposits in the research area using inexpensive image processing system.

1.3 Objectives of the present study

This research aims to answer the following question: how useful is multispectral (LANDSAT ETM and ASTER) datasets in identifying and mapping hydrothermal alterations associated with iron ore mineralization in the Sheini Hills, Ghana?

The objective therefore is to use remote sensing for

- The recognition of hydrothermal alteration zone within which the Sheini iron project resides
- The establishment of a template to identify hydrothermally altered areas from Landsat ETM and ASTER data

Carlos A. Torres., (2007) reported that although iron ore cannot be detected directly by any remote sensing method, the presence of iron oxides and iron hydroxides whose diagnostic spectral signatures, (in the visible/shortwave infrared portion of the electromagnetic spectrum) could be used as indicators for identification of hydrothermal alteration zones, which are associated with iron ore occurrences.

1. 4 Review of the study area

1. 4.1. Geographical location and size

The study area is in the Sheini-Sangba areas in the Northern Region of Ghana. This area is about 160 km east of Tamale the regional capital. Administratively, the Sheini area is within the Zabzugu-Tatale district. The concession area is approximately 398 km^2 and roughly within Longitude 0^0 26 E, in the west to the Ghana-Togo Border, and Latitudes 9^0 00 N to 9^0 20 N, on the Ghana Survey topographical field sheets 0800A2, 0900C4 and 0900D3 on 1:50 000 .

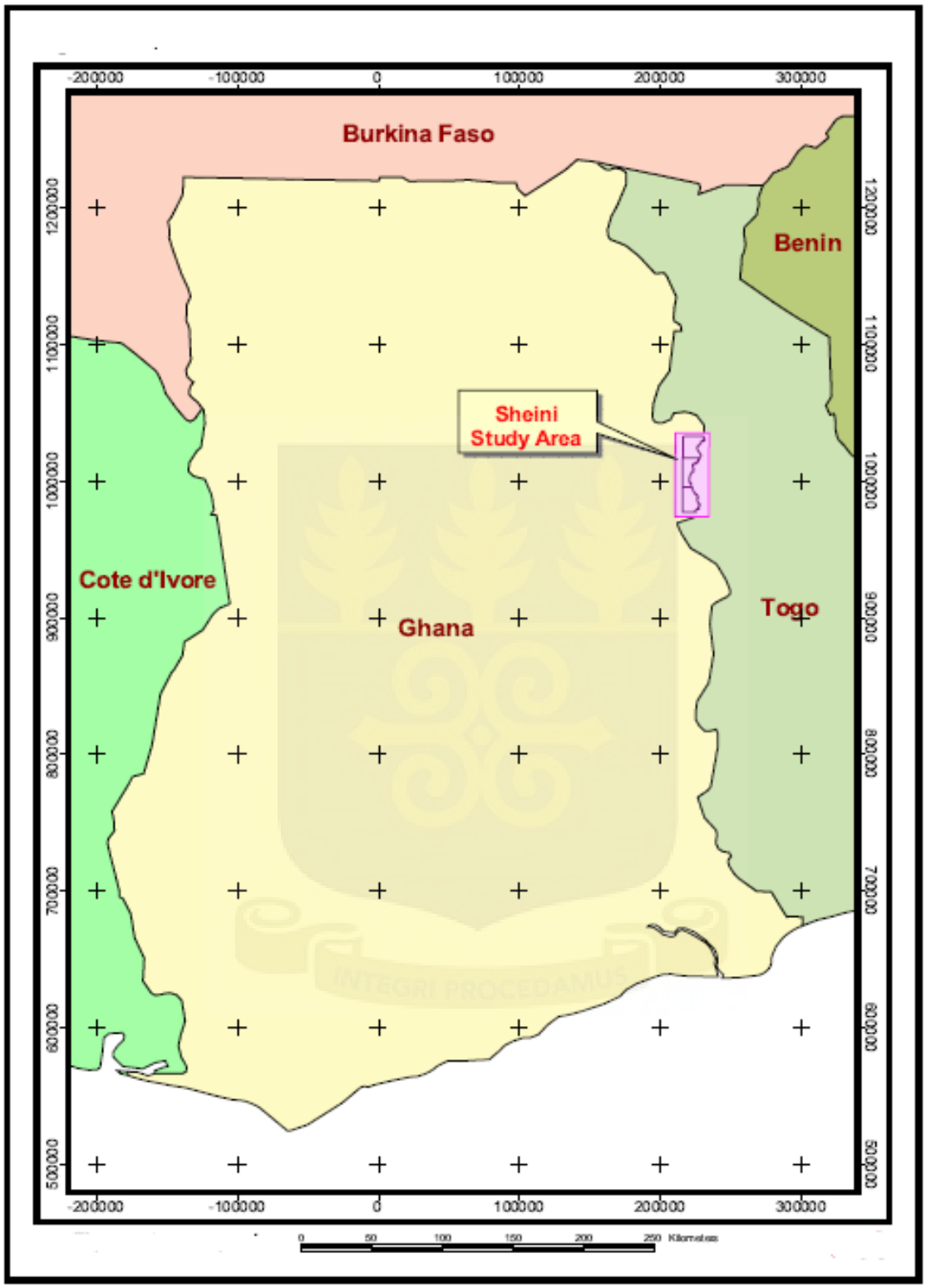

Figure 1: Location of the study area. **(**Cardero., 2012)

1.4.2 Physiography

The terrain of Northern Region reflects the geological setting of the area. The landscape around the city of Tamale is generally flat, and belongs to the soft sedimentary rocks of the Volta Basin that outcrop in the area. East of Tamale and the Oti River, small hills with elevations rising to approximately 150 m above sea level are common, indicating the presence of more resistive rock formations. The Oti River forms a broad valley with elevations of 80–90 m above sea level in the vicinity of the Sheini area. Close to the Togo border, the Sheini Project area is characterized by a series of broadly N-S trending ridges surrounded by slightly undulating savannah. The majority of the ridges, which trend approximately 30 km south from the Zabzugu–Sheini road, are related to thick sequences of ironstone and generally range from 150 m to 400 m above sea level. The ironstone typically forms sharp, narrow ridges with the development of scree slopes at the base commonly surrounded by large, flat areas of detrital material. (Henderson, K.J., 2012)

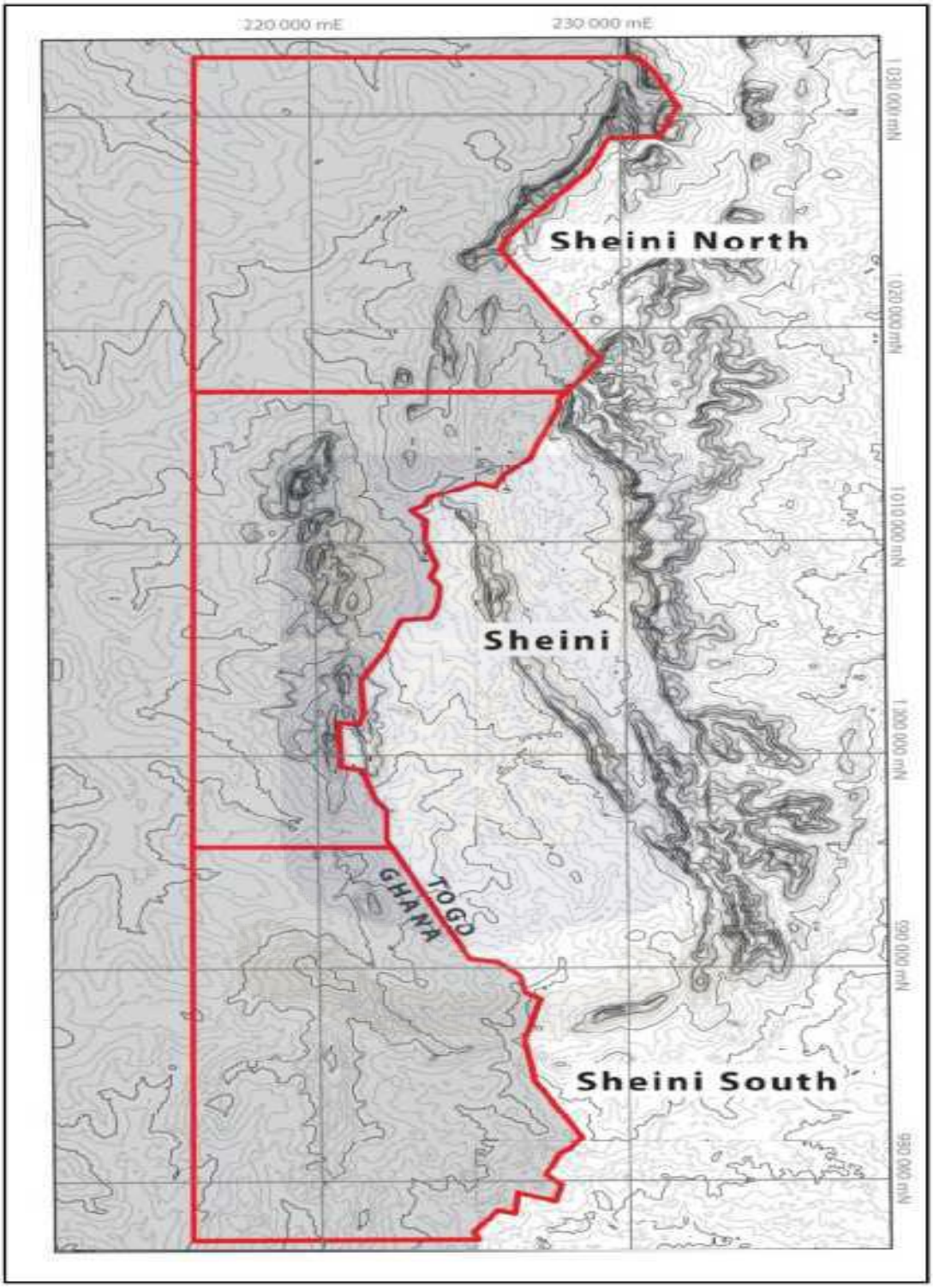

Figure 2: Topographical Map of the Study Area. (Cardero, 2012)

1.4.3 Rivers and drainages

All of the streams and rivers in the Project Area draining westward from the ridges at the Ghana-Togo border are tributaries of the Oti River, which flows southward into Lake Volta. The small streams and rivers in the Sheini area are seasonal and are dry from the end of January until the end of May. The Oti River flows throughout the year. (Henderson, K.J., 2012)

1.4.4 Vegetation

The vegetation in flat areas surrounding ridges features typical African semi-open savannah woodland, with baobab, mango, and acacia trees and a variety of bushes. Dense grass reaches a height of 4 m during the rainy season , and grasses, bushes, and trees surround streams and rivers year-8round . Farmers cultivate much of the land around villages and, as such, dry-brush and grass is typically burned from fields in December, following the rainy season. A variety of crops are grown, including: yam, cassava, guinea corn, millet, maize, hot pepper, tomato, and ground nuts. Small trees, bushes, and tall grasses vegetate the ridges. (Henderson, K.J., 2012)

1.4.5 Climate

The Northern Region of Ghana is located in the savannah belt with a typical hot sub-Saharan climate. There are two major seasons: dry and wet. The dry season is locally called Harmattan after a dry Sahara wind that blows from the northeast from the end of November to March and brings fine dust, often decreasing the visibility during the day. The wind affects the climate mainly in northern Ghana where it decreases the air humidity and creates hot days and cool nights. The days during the dry season are usually cloud-free. Mornings are colder and sometimes humid with fog. The temperature at night is 15°C–20°C, but rises rapidly by midday to highs of 45°C. The lowest temperatures at night in the Sheini area are in January. The hottest

days occur during March and April. The first thunderstorms, followed by short but intense rain, commence in the second half of March. (Henderson, K.J., 2012)

The rainy season extends from the end of March to late October or early November. The temperatures vary between 25°C and 45°C, with daily highs frequently in excess of 40°C. The highest rainfall is between July and August when the average rainfall is about 1,000 mm–1,300 mm. With upgrades to local roads ongoing and a proper maintenance schedule instituted, climatic conditions are not expected to adversely impact exploration activities in the project area. (Henderson, K.J., 2012)

CHAPTER TWO

GEOLOGICAL SETTING AND MINERALIZATION

2.1 Literature review

Different authors have investigated the application of GIS and Remote Sensing in the field of mineral exploration and their works include the following: Chica-Olmo et al., (2002) applied Remote Sensing techniques and spatial data analysis through GIS in a mineral exploration context to identify gold-rich potential areas in SE Spain. Remote Sensing results were integrated, in conjunction with existing maps and data from mineral exploration surveys; into the GIS as vector or raster layers. The result confirmed the usefulness of this integrated methodological approach as an effective tool to assess mineral potential in the studied region. Chandrasekar et al., (2011) investigated heavy-mineral deposits using multispectral satellite data to map out the mineral deposits in South Tamil Nadu Coast of India; and then mapped out minerals which show significant variation in reflectance at different spectral bands, which has opened up new areas for inland heavy mineral exploitation and leads to eco-friendly exploitation of natural resources along the study area. It also illustrated the high potential of multispectral satellite data for exploration and mapping of mineral resources. Asadi et al., (2001) used aeromagnetic data, Landsat Thematic Mapper (TM), geological and mineral occurrence data to map the gold potential at Takab area of Northwest Iran.

Kianfeng et al., (2007) in their work used Advanced Spaceborne Thermal Emission and Reflection Radiometer (ASTER) radiance data to map Lithologies related to gold deposit in the South Chocolate Mountains area, California; then compared different methods for extracting mineralogic information from ASTER data and also compared the remotely derived maps to the

mapped field geology, and used the ASTER data to map minerals and lithologies related to gold exploration. Andrada-de-Palomera (2004) used Landsat ETM+ and ASTER image to map the potential gold areas in the Deseado Massif, Southern Argentina; followed by extracting the mineralogical indicative features from the ASTER data and the indicative hydrothermal alteration from Landsat data and these data were integrated with other geologic data such as lineaments. Kaisser et al., (2004) used Landsat ETM+ image to map potential gold deposit in WadiAlaqi District in Egypt; as well as the band ratio technique (i.e., mineral ratio and hydrothermal ratio) to discriminate different lithology types for geological mapping.

In 2012 a Landsat ETM+ and an ASTER image, centered on the Sheini Hills project area in east-central Ghana, were acquired and processed. A 24 km (E-W) by 61 km (N-S) image extract was interpreted at up to 1:25,000 scale in order to define the structural framework of the area by Murphy Geological Services from Ireland. This, together with ASTER and Landsat derived alteration anomalies, was used to generate iron ore exploration targets. Eleven exploration targets were identified within the Sheini project area. The targets were based on a number of criteria including the presence of major belt parallel thrusts and transverse faults, fault intersections, branching along major faults, presence of iron formations and ferricretes, thrust repetition and folding of iron formations and the presence of ASTER/Landsat ETM+ derived alteration anomalies.

2.2 Regional geology and tectonics

The Sheini Hills project area is located to the east of the West African Craton, within a southern portion of the Trans-Saharan belt known as the Dahomeyan Belt (Kröner and Stern, 2004). The regional geology of the Sheini area which has been described by several workers including Crook (1956), Jaques (1958) Kesse (1985) is shown in Figure 3. From recent geological mapping work conducted by the Geological Survey of Ghana (Geological map of Ghana, 2010 1: 1, 000, 000), the ore zone is within the northern sections of the Buem Structural unit of the Dahomeyides outcropping in Ghana

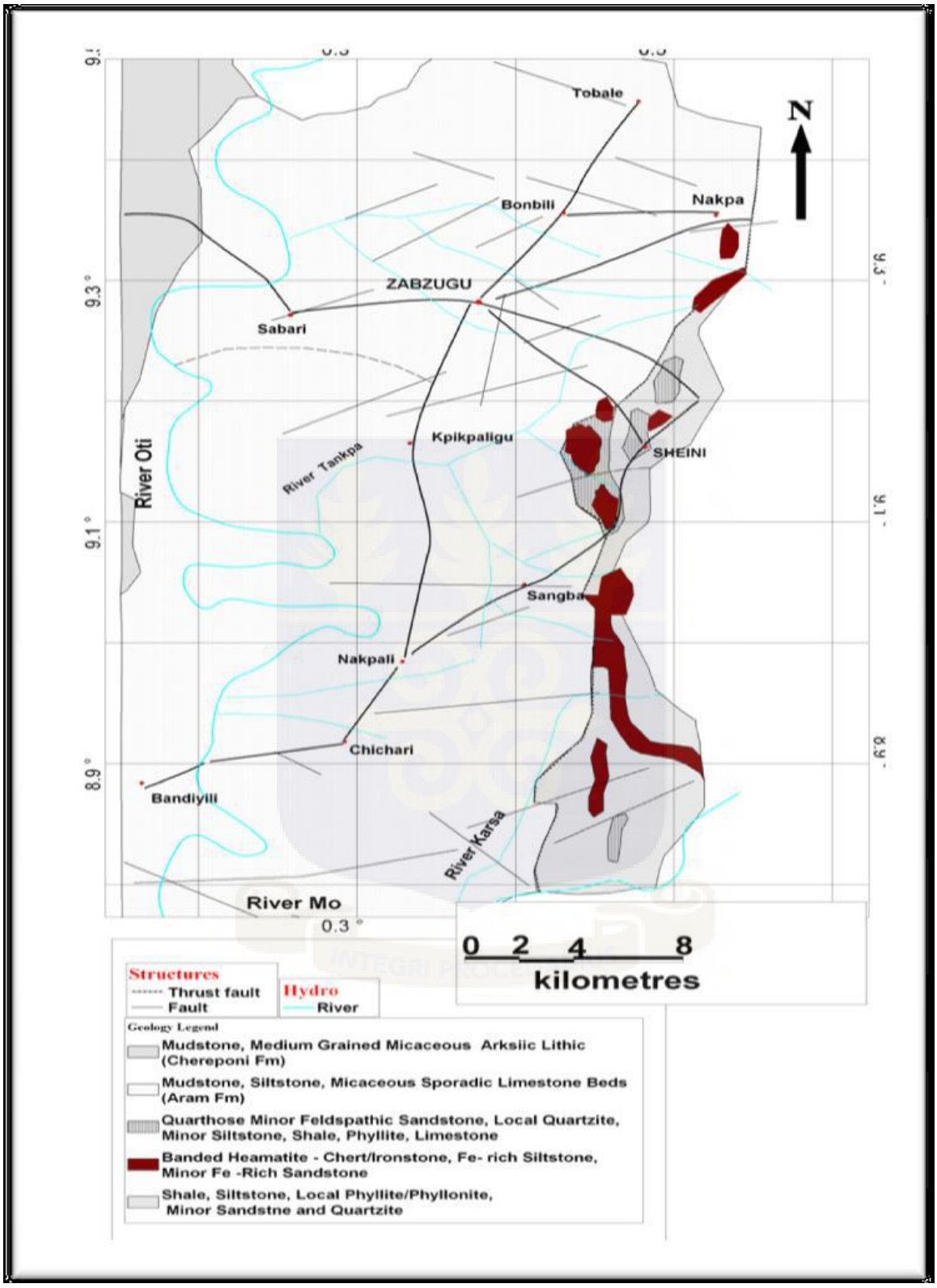

Figure 3: Regional Geological map. (Nude et al.,2011)

The major lithologies of the Buem units in the area comprise quartzose and feldspathic sandstones, some quartzites with shales, phyllites, siltstones and minor limestone. These units form prominent N-S trending narrow hills separated by low grounds. (Nude et al.,2011) On the west of these units, the Buem has been mapped to be in tectonic contact with the Neoproterozoic middle Voltaian of Oti-Pendjari group, where it is thrusted over the Voltaian. The Voltaian lithologies here include mudstones, siltstones, and occasional limestones, all belonging to the Afram formation. The rocks of the Buem units in the project area are noted to follow the regional structural trend of N-S; the rocks are sheared and deformed and contain variegated ferruginous tillite horizons that host the iron ore. The major lineaments in the area are NNE-SSW with minor N-S ones. The origin of the ferruginous tillites is uncertain, although iron oxide alteration of the original tillites is a possible candidate. It is also possible that a failed basaltic volcanism which never reached the surface may have introduced iron oxide into the rocks. This assumption is based on the occurrence of similar ferruginous rocks further south of the area in the Pasa-Adomakuma areas with volcanic rocks of basaltic-andesitic compositions. Nude et al., 2011

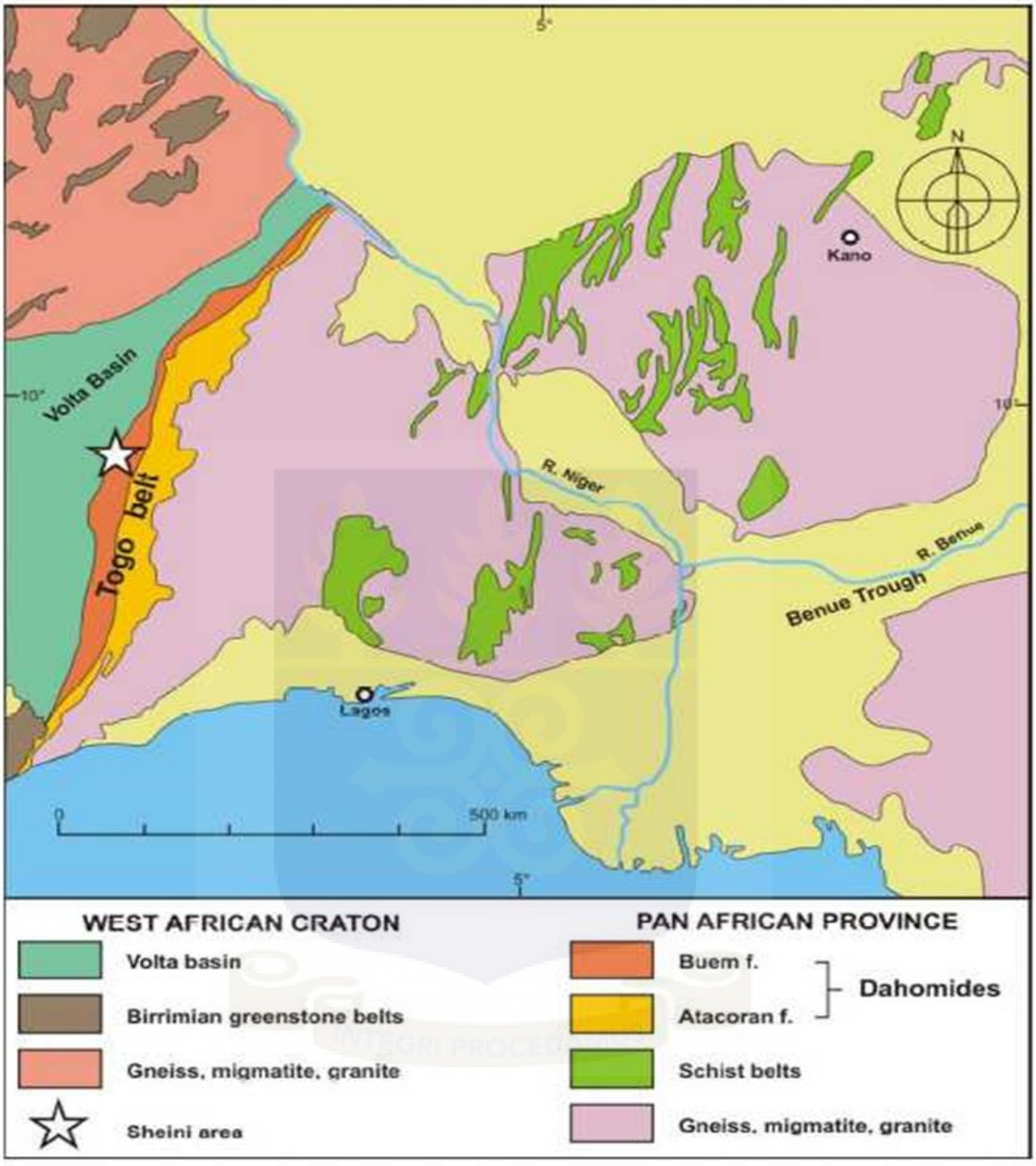

Figure 4: Summary geological map of the Volta Basin and Togo Belt (from Henderson, 2012)

2.3 Geology of the study area

The Sheini Hills Project Area is located at the boundary between the Buem Structural Unit (BSU) and underlying Voltaian Supergoup. Ironstone, thought to belong to the base of the BSU, forms a series of ridges which trend roughly north-south. However, the exact position of the border between the BSU and Voltaian Supergroup is unclear due to poor outcrop distribution east of the Ironstone ridges. The closest observed outcrops belonging to the Voltaian Supergroup are near flat lying greenish-grey to white sandstone, arkose, greywacke and mudstone, likely of the Oti-Pendjari Group, which outcrop proximal to the Oti River approximately 20 km west of the project area. Similar rocks are likely located immediately west of the BSU ridges in the project area, however, the flat-lying lowland, sub-horizontal bedding, and Phanerozoic cover prevents outcrop recognition. Probable Voltaian Supergroup sediments are intersected at the end of several boreholes drilled during the recent exploration programme conducted by Emmaland Resources. In drill core these rocks are grey-colored, fine-grained sediments with sub-horizontal bedding and cross-cutting carbonate stringers with local disseminated pyrite, similar to the lithological unit observed proximal to the Oti River. This lithology resides beneath the iron formation, footwall diamictite, and footwall black shale, and forms local down-stepping terraces west of the BSU ridges. Henderson, K.J., 2012

The BSU belt is approximately 5-15 km wide, and is present in all three prospecting licenses. In the project area, the BSU has been divided into three basic lithologic units:

- Hanging wall formation (mudstone, greywacke and sandstone).
- Buem iron formation (banded and granular iron formation).
- Footwall formation (diamictite, sandstone, greywacke and quartzite).

Iron-rich sedimentary rocks are typically classified as ironstones, or as iron formations. Sedimentary rocks must contain greater-than 15% iron to be considered iron-rich (Bekker et al., 2010). Ironstones are typically Phanerozoic in age, or less than 540 Ma, while iron formations are typically Precambrian in age (4600-590 Ma). Iron formations are further classified as either banded iron formation (BIF), or granular iron formation (GIF). BIF typically displays well developed laminations with layers alternating between iron-rich sediments, and chert, sandstone, mudstone, or siltstone. GIF typically lacks any continuous banding, although cross-bedding and other discontinuous layering may be present. BIF can display granular aspects. Cardero., 2012

The iron-rich rocks near Sheini typically contain greater than 30% iron and display two typical primary textures including: 1) laminated/micro-banded iron-rich mudstone with alternating bands of silicified sandstone laths (typically 1 cm thick by 2-3 cm long) and irregular lenses/bands of chert, and 2) massive, granular iron-rich sediments with polymictic clasts (typically granitic, pegmatitic, and schistose). The iron-rich rocks at Sheini exhibit both BIF and GIF properties and are hereto referred to as the Buem iron formation. Neoproterozoic rocks in the project area are covered by younger Cenozoic clastic sediments that form flat lying deposits surrounding the north–south trending ridges. Of greatest economic significance are a series of irregular shaped detrital iron deposits, up to 29 m thick, which occur at the base of BSU ridges. The detrital deposits are predominantly composed of clasts of iron formation derived from the Buem iron formation, cemented by a sandy hematitic clay matrix. The surface of these deposits is typically covered by a thick layer (1-5 m) of hard ferricrete. (Cardero, 2012). Detailed descriptions of the lithologic units are presented below:

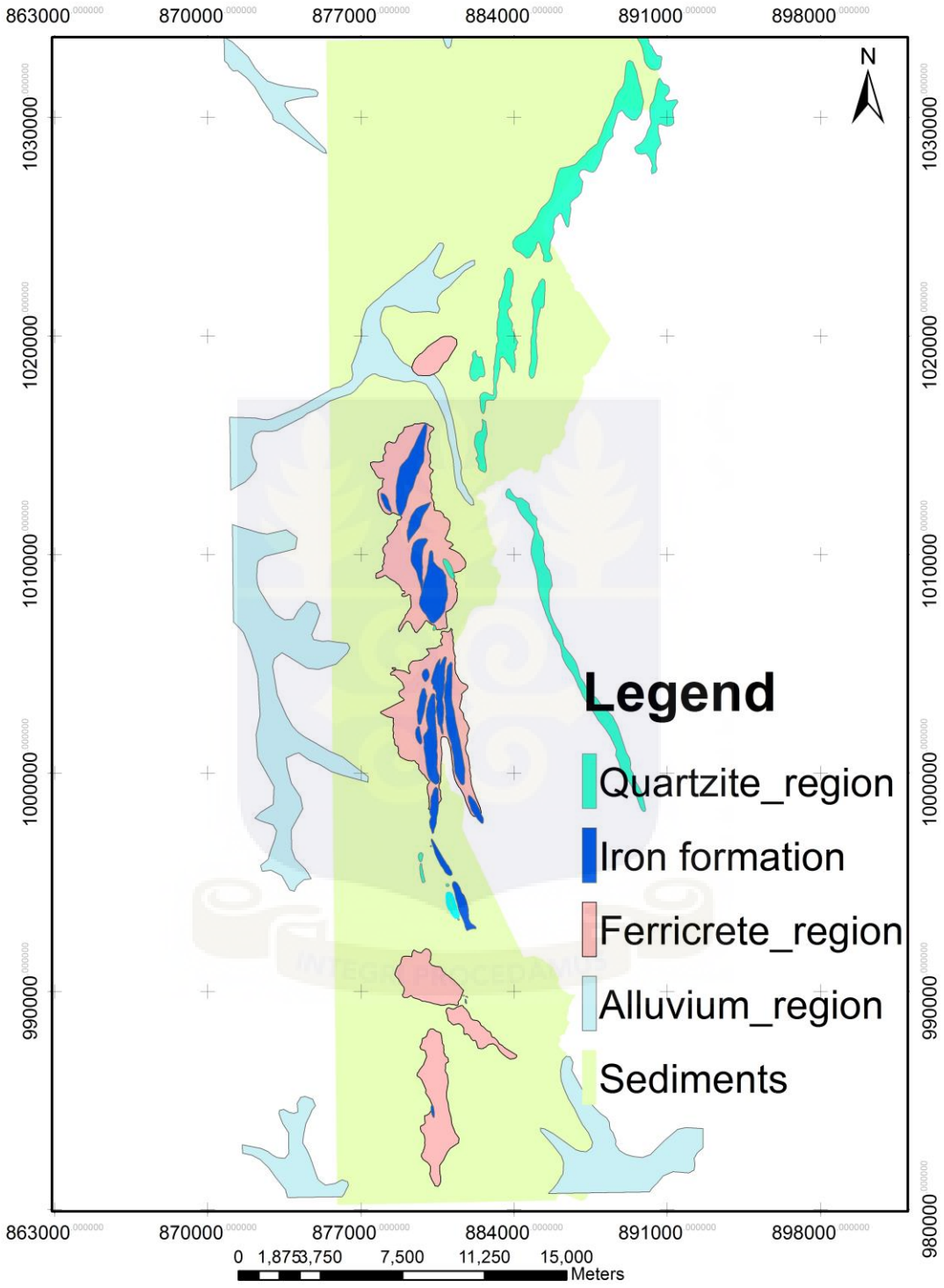

Figure 5: Geological map of the study area

2.3.1 Hanging wall

Hanging wall rocks are largely intersected in the central portions of long, narrow synclines. Surface outcrops are rare and most observations are from drill-core only, although their presence at surface can be marked by soft, sandy, light tan-colored soil, and local saprolitic profiles in road cuts. Hanging wall drillhole intersections are typically less than 60 m thick, however intervals of up to 260 m in thickness are intersected between folded overturned layers of iron formation. Prevailing lithologies include greenish-grey colored, very fine-grained to fine-grained, poorly sorted sandstone with interbedded siltstone and mudstone. Sandstone is dominantly composed of subangular quartz with minor grains of chert, feldspar and muscovite. Siltstone and mudstone contain abundant phyllosilicates (muscovite, chlorite). Locally, thin (0.5 to 2.0 m thick) lenses of white colored, fine-grained, massive quartzite (which are seen to outcrop locally) have been observed with common pyrite aggregates along fracture planes. Rare, thin (0.1 to 1.0 m thick) conglomeritic zones are also occasionally present. Sub angular to sub rounded clasts composed of siliciclastic rocks (sandstone, siltstone and mudstone) and typically 0.5 to 2 cm in diameter have also been observed in the hanging wall, but are not a prominent feature. (Cardero, 2012)

Hanging wall rocks are typically very clean with minimal alteration, however, locally iron oxide alteration has been observed at the contact between hanging wall and the iron formation. These alteration zones, which are generally localized to the northern area of the recent exploration programme, are typically several meters thick (locally up to 30 m and are defined by brown sandy siltstone and/or mudstone with partial replacement of the matrix by iron oxides (haematite) and iron hydroxides (haematite, goethite). Assays from the recent exploration programme show these hanging wall alteration zones to contain 10 to 15% iron. (Cardero, 2012)

2.3.2 Iron formation

The Buem iron formation forms a thick (29 to 120 m) sequence comprising both banded and granular iron formation immediately above the footwall diamictite, and overlain by a sequence of fine-grained clastic hanging wall sediments. The Buem iron formation is the dominant formational unit of the brachysynclinal structures. The thickness of the iron formation is approximately consistent within each brachysynclinal structure, but generally increases towards the north. Recent exploration indicates that the banded iron formation is more prevalent than granular iron formation in the northern area of the recent exploration programme. (Cardero, 2012)

2.3.2.1. Banded Iron Formation

BIF in the Sheini Project area is typically brick red to dark red and formed by mm to cm scale bands and laminations of sandstone laths and fine grained hematite. Sandstone laths are typically up to 1 cm thick by 2-3 cm wide and commonly display silicified rims with partially eroded cores, surrounded by haematite-mineralization. Banding is observable in both outcrop and drill core, however, it is most easily observed through petrographic analysis. Petrographic inspection of BIF indicates that bands and laminations predominantly consist of upward-fining, graded-bedding between quartz and haematite with quartz grains commonly forming the base of laminations and bladed haematite increasing in abundance toward the top. Quartz grains are typically subangular and vary in size from approximately 40 μm to 1 mm. Haematite forms an irregular mesh composed of blades that are 30 to 100 μm wide by 3 to 5 μm thick. (Cardero, 2012)

Locally, the BIF is cross-cut by numerous thin veinlets of quartz, amorphous silica, secondary haematite, chlorite (chamosite) and siderite. Siderite and amorphous silica are also common near the base of the Buem iron formation. Near the base of the Buem iron formation, siderite and amorphous silica lenses replace BIF along apparent bedding planes, which are postulated to be the result of post-formational tectonic and hydrothermal processes. Irregular shaped jasper-like cherty lenses are also irregularly dispersed throughout the BIF. (Cardero, 2012)

2.3.2.2. Granular Iron Formation

GIF is typically brick red to dark red-brown, comprising mm to m scale subangular to subrounded lithic clasts set in a haematitic matrix. Clasts are largely composed of granite, pegmatite, and schist, with lesser sandstone, quartzite, and mudstone. At present, clasts of iron formation have not been observed. Similar to haematite of the BIF, the haematitic matrix of the GIF consists of an irregular haematitic mesh formed by blades of haematite, measuring 30 to 100 μm and 3 to 5 μm thick. Haematite fills free space in lithic clasts and replaces fine-grained phyllosilicates (muscovite and chlorite). Quartz grains similar to those in the BIF are also present. (Cardero, 2012)

2.3.3 Footwall.

The footwall to the Buem iron formation generally comprises poorly sorted, coarse-grained sediments. Footwall rocks are rarely found in outcrop due to a low resistance to natural weathering processes. Most observations are made from drill core and rare saprolite profiles exposed in fresh road cuts during recent exploration activities.

The dominant footwall lithology is a distinctive pale to dark grey, medium to coarse grained

sandstone with mm to m scale angular, subangular, and subrounded clasts which comprise 15 to 30% of the unit. Clasts are predominantly composed of granite, pegmatite, and mica schist, with lesser amounts of quartzite, sandstone, and mudstone. The matrix dominantly consists of grains varying in size from silt to coarse sand. Thin section analysis indicates the presence of muscovite, chlorite and rare feldspar in the matrix, in addition to rare accessory pyrite and rutile and trace levels of volcanic glass. This rock is typically massive with no visible bedding. Local horizons of greywacke and fine-grained sandstone are occasionally characterized by graded bedding with fine laminations largely composed of muscovite and chlorite. Local cross-bedding has also been observed. (Cardero, 2012)

The footwall sandstone is commonly oxidized at the contact with the overlying Buem iron formation. Fine-grained aggregates of iron oxide (haematite) and iron hydroxide (goethite, limonite) fill free space between grains of the poorly sorted sandstone. Thin section analysis of altered zones show that only phyllosilicates (muscovite, chlorite, etc) are replaced, leaving other minerals and larger clasts unaltered. The alteration profile varies in thickness from several cm to greater than 50m. Distinct (cm scale) contacts are observed where alteration is thinnest (typically in the southern area of recent exploration), while very diffuse, gradational contacts exist in wider zones of alteration (northern area of the recent exploration). The altered sandstone is defined by red-brown color and typically contains 10 to 20% iron (based on recent assay analysis). (Cardero, 2012)

Historical reports (Jacques, 1958; Bobrov & Pentelkov, 1964) and scientific papers (Wright et al., 1985) describe this rock as unaltered tillite due to its similarities with known tillites forming

the base of the Oti-Pendjari Group (Wright et al., 1985). These tillites are known to be associated with striated clasts most likely of glacial origin. However, such striations have not been observed during the recent exploration programme. Diamictite is a sedimentary rock consisting of various lithified, unsorted to poorly sorted, terrigenous materials with various clast and grain sizes and is associated with numerous geological processes and environments (glacial, volcanic, marine, tectonic, and erosional). Diamictite is present in the footwall to the iron formation in the entire area of recent exploration. (Cardero, 2012)

2.3.4 Detrital iron deposits

Detrital iron deposits form extensive flat-lying platforms adjacent to ridges in the project area. These platforms tend to be sub-circular and are likely paleo-alluvial cones occurring where ridges of iron formation are cross-cut by major fault zones. Recent drilling shows the detrital iron deposits to be of variable thickness, ranging from 1 to 29 m thick.

Typically, the detrital iron platforms are characterized by a succession comprising:

- An upper hard ferricrete surface, generally 1 to 5 m thick.
- A central zone of gravel, both consolidated and unconsolidated with clasts of iron formation set in an iron-rich, sandy, clay matrix.
- A lower thin (< 0.5 m thick) layer of secondary fine grained ironstone.

Brown to red, mm to m scale clasts derived from the Buem iron formation, are present throughout the upper ferricrete zone and central consolidated gravel). Detrital iron matrix consists of yellow-orange to red colored iron-rich, sandy clay. Locally, a thin layer of ironstone exists at the base of detrital iron deposits. It is generally less than 0.5 m thick and contains no clasts. It is postulated that this ironstone layer may be the result of supergene enrichment from

surface waters percolating through iron-rich gravels above. The lower contact of detrital iron deposits is usually defined by several metres of iron sulphate (jarosite) alteration, which likely formed in response to chemical weathering of bedrock by iron-rich acidic fluids. (Cardero, 2012)

2.4 Mineralization

Mineralization predominantly comprises bladed hematite with lesser iron hydroxides (goethite, limonite), and very rare magnetite and pyrite grains. Primary iron mineralization is largely confined to thinly banded, laminated iron formation and granular diamictic iron formation, which are commonly interbedded. Granular iron formation is more consistently interbedded with banded iron formation in the southern area of recent exploration, while banded iron formation dominates to the north. The iron-rich rocks near Sheini clearly reside within strata that have been thrust over the Voltaian Supergroup to the west during the Panafrican orogeny (BSU). The GGSD, Accra, Republic of Ghana (2009) suggests that the BSU is time-equivalent to the Kwahu-Morago' Group (1000 Ma to 950 Ma) of the Voltaian Supergroup. Although no volcanic rocks have been found in the immediate vicinity of Sheini Hill the Geological Map of Ghana displays mafic and felsic volcanic units within the BSU (roughly 50 km south of the project area). The GGSD (2009) explains these volcanics to be related to 600 Ma rifting, and state that an intercontinental rift-zone developed within the Oti-Pendjari Group at what is now the eastern margin of the Voltaian Supergroup where the BSU resides. (Cardero, 2012)

In eastern Ghana, the Trans-Saharan belt is known as the Dahomeyide belt, and is said to contain ophiolitic (rift-related) mélange that was metamorphosed circa 614 Ma (Kroner and Stern, 2004). Jones (1990) concludes through analysis of geochemical and gravity data that

volcanic rocks residing within the BSU are related to rifting. As the Panafrican orogeny relates to the closing of an ocean basin and suturing of exotic blocks and the Sahara "metacraton" to the West African craton (Kroner and Stern, 2004), rocks of the Sheini Hills iron deposit must be related to an embryonic rift-basin developed from mantle plume events during the break-up of Rodinia, possibly forming in an aulacogen resulting from rifting between Amazonia and the West African craton (prior to the Panafrican orogeny). (Cardero, 2012)

Through new drilling data, it is believed that rocks of the BSU have been inaccurately attributed to be time-equivalent with the Kwahu-Morago' Group and more accurately resemble the basinal clastic glaciomarine sediments of the Oti-Pendjari Group. This would give the Buem iron formation an approximate age of 635 to 620 Ma, roughly coincident with the Marinoan glaciation. (Cardero, 2012)

CHAPTER THREE

METHODOLOGY

3.1 Remote sensing data and software

In this study, remotely sensed multispectral datasets comprising LANDSAT Enhanced Thematic Mapping (ETM+) and Advanced Space borne Thermal Emission and Reflection Radiometer (ASTER) level 1 A images were processed. The primary criteria for selecting ETM scenes to process were that they had to be cloud free and capture dates are very important considering vegetation when working in Sub Saharan areas like the Sheini Hills. The LANDSAT TM image with the path 193, row 054 was acquired on February 4, 2000 and the ASTER 0401301032530402090385 on the 30th January 2004. Other datasets includes a geological map. The Landsat data was downloaded from the USGS GLOVIS database (http://glovis.usgs.gov/).The ASTER data were donated by Murphy Geological Services.

The Landsat ETM+ image was downloaded as a pre-corrected orthorectified image and contains a total of 9 bands; 7 in the Visible and Near-Infrared (VNIR), 1 in the Thermal Infrared (TIR), region of the electromagnetic spectrum, and 1 panchromatic channel (band 8). Spatial resolution is 15 m for the panchromatic band, 30 m for VNIR bands, and 60 m for the TIR bands. The ASTER image has 14 bands; 3 bands in the (VNIR), 6 bands in the Short Wave Infrared (SWIR), and 5 bands in the (TIR) regions, with a spatial resolution of 15 m for VNIR, 30 m for the SWIR; and 90 m for TIR bands. A complete description of LANDSAT ETM+ and ASTER is illustrated in Table 1. Digital processing of these multispectral images has been achieved by the use of ArcGIS software version 10.0 and Erdas ER mapper software which are all complete digital processing programs capable of carrying out preprocessing, enhancement, transformation, and classification of remote sensing images in order to extract spatial and spectral information that

are related to geology, such as lithology and hydrothermal alteration.

Table 1: Comparison of spectral bands between ASTER and Landsat 7 (ETM+)

ASTER				Landsat-ETM		
	Band Number	Spectral range (µm)	Spatial resolution (m)	Band Number	Spectral range (µm)	Spatial resolution (m)
VNIR			15	1	0.45 – 0.52	30
	1	0.52 – 0.60		2	0.52 – 0.60	
	2	0.63 – 0.69		3	0.63 – 0.69	
	3	0.76 – 0.86		4	0.76 – 0.90	
SWIR	4	1.60 -1.70	30	5	1.55 – 1.75	
	5	2.145 – 2.185		7	2.08 – 2.35	
	6	2.185 – 2.225				
	7	2.235 – 2.285				
	8	2.295 – 2.365				
	9	2.360 – 2.430				
TIR	10	8.125 – 8.475	90			
	11	8.475 – 8.825				
	12	8.925 – 9.275				
	13	10.250 – 10.950		6	10.4 – 12.5	60 (ETM7)
	14	10.950 – 11.650				120 (TM5)

3.2 Processing techniques

This project is concerned with the processing of remotely sensed images for the purposes of alteration mapping, and integration with other datasets in a GIS environment. Image processing methods are designed to transform multispectral image data format into an image display that either increases contrast between interesting targets and the background or yields information about the composition of certain pixels in the image. The enhancements techniques, which have been applied in this study, included color composite, band ratioing, and principal components analysis (PCA).

3.2.1 Color composite images

Satellite images for a given scene are captured in black and white bands. The first three LANDSAT bands (1, 2, and 3) correspond to the blue, green, and red portions of the visible spectrum, which are captured as gray-scale images, together with ETM+ bands 4, 5, 6,7, and 8 also. A composite image is generated by blending information from two or more bands. When an image contains bands in an order corresponding to the red, green, and blue portion of the visible spectrum, then it is called a natural or true color composite image (http://calview.casil.ucdavis.edu). When an image is created from a combination of one or more non-visible EM spectra or non-true color composite images, then it is known as a false color composite (FCC) image. It is possible to create a color composite image by blending visible and infrared bands or by using infrared bands only. Interpretation of FCC images depends on the manner in which the bands are assigned to the three principal colors used for the image display. The production of color composite images is based on known spectral properties of rocks and alteration minerals in relation to the selected spectral bands. For instance, LANDSAT ETM band 7 is used primarily for mineral and rock discrimination, whereas bands 3 and 4 are primarily

used for vegetation monitoring.

Spectral analysis exploits spectral properties of rocks in order to interpret lithological variations or rock alterations that are expressed as variations in color intensity values within color composite images. A display of FCC images in a color scheme that is well balanced among the display colors is known as contrast-enhanced False Color Composite, which is meant to provide better overview of the area of investigation. Contrast enhancement of images is a widely used procedure by which brightness values of an image (0-255) are stretched such that light-toned areas appear lighter and dark areas appear darker, making visual interpretation easier. Several FCC images of the study area have been generated by combination of various bands displayed as red, green, and blue RGB, using both LANDSAT ETM and ASTER images. (Vincent, 1997)

i. LANDSAT ETM+ Images

LANDSAT ETM+ band combinations have been used to extract lithology in this study .A color composite in Red Green Blue (RGB) image with high standard deviation and less redundancy is chosen to void duplication. The most informative band combination should include one visible (1, 2, and 3), one NIR (4), and one SWIR (5,7 and 8). (Vincent, 1997)

ii. ASTER data Images

For Aster, there are a total of 364 color combinations derived from its 14 bands. The best 3-band combinations which was used for lithological discrimination, are selected by a process similar to that mentioned above in the case of LANDSAT ETM+. (Vincent., 1997)

3.2.2 Band ratios (BR)

Band ratioing is a technique used in remote sensing to effectively display spectral variations (Vincent and Thompson, 1972; Goetz et al, 1975). Ratio images enhance the contrast between materials by dividing the digital number (DN) value of one band by the digital number (DN) value of another band in a reflectance curve. Ratio images may correlate to one or more surface materials such as lithologic types and vegetation density (Crowley et al., 1989; Sabine, 1997; Gupta, 2003). The band ratio technique has been widely used to extract hydrothermal mineral information in the analysis of Landsat MSS, TM, ETM and ASTER image data. (Perry, 2004)

There are many types of band ratios in use, depending on the purpose of their application (e.g., lithology or alteration discrimination). Similarly, the choice of bands depends on their spectral reflectance and positions of the absorption bands of the mineral being mapped. For instance, to enhance a specific alteration mineral that hosts a distinct absorption feature, the most unique spectral ratio for that mineral is employed. An example is the LANDSAT ratio B5/B7 that is needed to enhance clay-carbonate-sulfate-mica minerals relative to the others. The greater utility of the spectral bands ratioing can be obtained when applying bands from inside and outside a wavelength region of spectral reflectance maximum or minimum of a particular target. (Vincent, 1997). Spectral ratios of spectral bands that are separated widely in wavelength can also be helpful when the mineral of interest has a relatively unique overall shape of the reflectance spectrum, involving both visible and shortwave infrared bands.

For iron minerals (e.g., gossans) the reflectance in LANDSAT ETM band 1 (0.45-0.52 μm) is weaker in comparison to band 3 (0.63-0.69 μm) which is stronger, so the band ratio 3/1 is suitable for discriminating iron oxides (Fig. 6). Likewise, clay minerals such as kaolinite,

montmorillonite, and alunite exhibit low reflectance in band 7 (2.08-2.35 μm) and high reflectance in band 5 (1.55-1.75 μm); hence, the band ratio 5/7 would have a characteristic bright signature for clay alteration zones (Fig. 7)

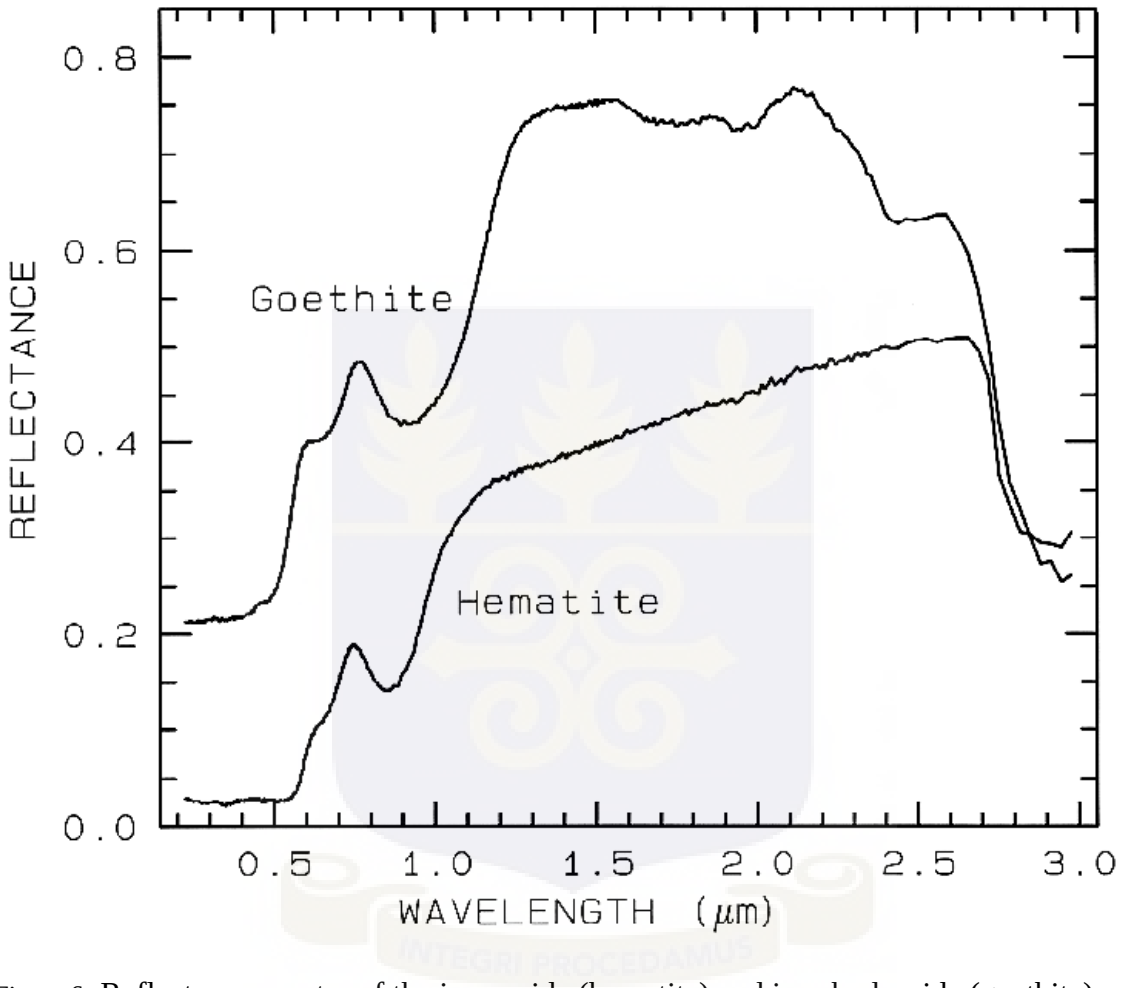

Figure 6: Reflectance spectra of the iron oxide (hematite) and iron hydroxide (goethite) after Clark et al., 1993

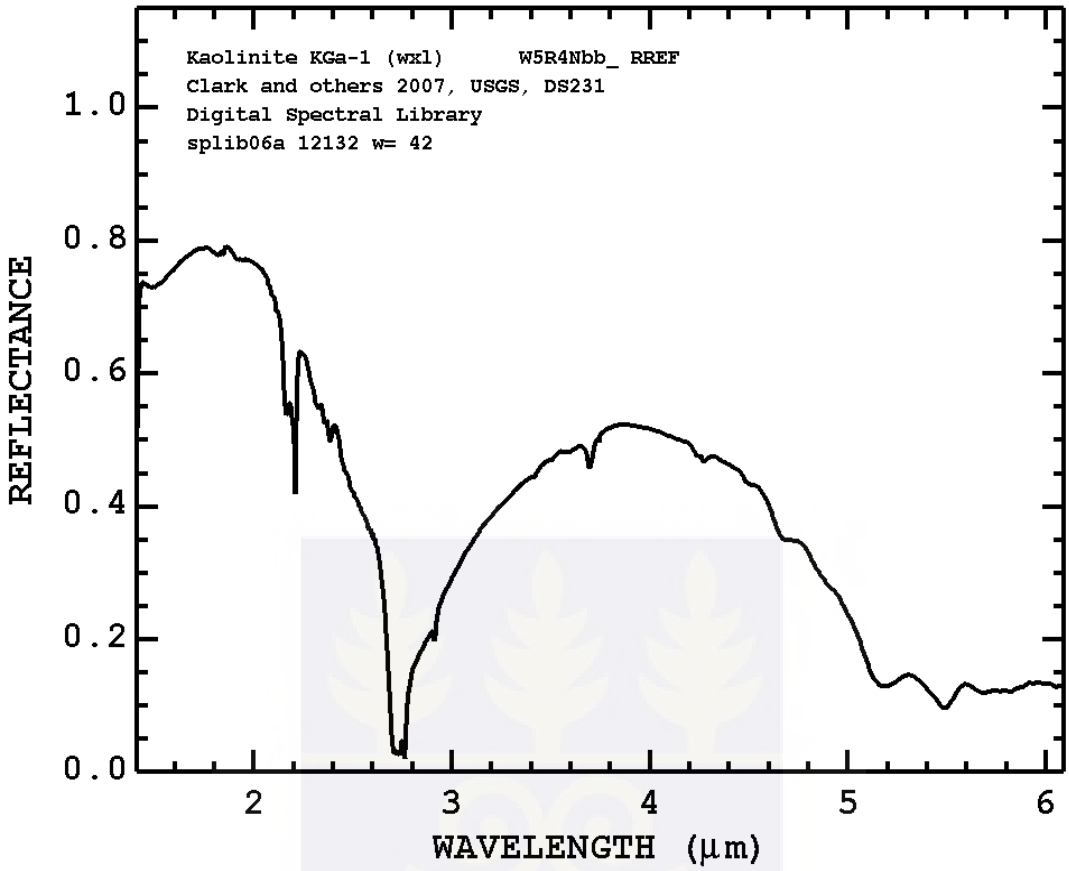

Figure 7: Reflectance spectra of kaolinite (1.5-6.0 µm) after Clark et al., 1993

i. LANDSAT ETM+ Images

Landsat ratio operation provides unique information that is not available in any single band which is very useful for disintegrating the surface materials (Jensen, 1996). The band ratio images are known for enhancement of spectral contrasts among the bands considered in the ratio operation and have successfully been used in mapping of alteration zones (Segal, 1983). From the theoretical knowledge of mineral's spectral properties, it is well recognized that the Landsat ETM bands ratios of 3/1, 5/7, 5/4 are analyzed for iron oxides, hydroxyl bearing minerals, ferrous oxides, respectively.

ii. ASTER data Images

Because ASTER has 14 spectral channels, more ratio images, and therefore more lithologic indices, more accurate results can be derived from ASTER data. The optimal band selection for ratio images depends on the spectral properties of the surface material of interest and its abundance relative to other surface cover types (Sabine, 1999). The spectral bands of the ASTER SWIR subsystem were designed to measure reflected solar radiation in one band centered at 1.65 μm, and five bands in the 2.10–2.45 μm region in order to distinguish Al-OH, Fe, Mg-OH, H-O-H, and CO_3 absorption features. ASTER band 1 and band 3 absorption features detect mainly Fe-oxides; ASTER bands 5 and 6 absorption detect Al–OH caused by clay minerals, alunite and/or muscovite/sericite, ASTER band 7 detects Fe–OH caused mainly by jarosite and/or Fe-muscovite and ASTER band 8 detects Mg–OH caused mainly by chlorite, epidote and/or carbonates (CO_3). Several investigators have documented identification of specific minerals, such as calcite, dolomite, and muscovite, as well as mineral groups, through analysis of ASTER data (Rowan and Mars, 2003; Rowan et al., 2003; Mars and Rowan 2006; Sanjeevi, 2008).

3.2.3 Principal components analysis (PCA)

The principal component transformation is a multivariate statistical technique that selects uncorrelated linear combinations (eigenvector loadings) of variables. Each successively extracted linear combination, or principal component (PC), has a smaller variance. The principal component analysis is widely used for alteration mapping in metallogenic provinces. Loughlin WP (1991). Through the analysis of the eigenvector values, it allows identification of the principal components that contain spectra information about specific minerals, as well as the contribution of each of the original bands to the components. This technique indicates whether

the materials are represented by bright or dark pixels in the principal components according to the magnitude and sign of the eigenvectors loadings. The technique can be applied on ETM+ and ASTER data. (Crosta et al., 1993)

The overall goal of PCA is to reduce the dimensionality of data set, while simultaneously retaining the information present in the data. In this study, the Crosta technique (Crosta et al., 1993) was applied for PCA, whose important aspect is the prediction of whether the target surface type will be highlighted by dark or bright pixels in the relevant PC image. The produced number of output PC bands is the same as the number of the input spectral bands. The first principal component (PC1) is a vector in the direction of the maximum variance of pixels in the scene. PC1 contains most of the data variability, dominated by brightness differences caused by variation of surface topographic slope directions, with respect to the sun position, and often displays important structural information. The second principal component (PC2) contains the second most variability, and is orthogonal to PC1 in n directional space. It emphasizes the spectral difference between the visible and the Infrared spectra. The third PC contains the third most variability and is orthogonal to the other two PCs, and so forth. The highest PC component contains all of the remaining variance and separates the most spectrally unique pixels (objects) from the rest of the pixels in the scene. Each subsequent PC removes the maximum amount of variance, which becomes smaller as the order of the PC increases (Vincent, 1997).

Any three principal components can be blended into a color composite image that contains information from all n bands, a characteristic that might help in displaying the widely distribution of alteration zones in a study area, which would not be revealed by a color composite

of any three single-band images. Also, PC color composite images appear more colorful than the respective spectral color composite images, due to their uncorrelated components.

3.2.3.1. Feature Oriented Principal Components Selection (FPCS)

Crosta and McM-Moore (1989) describe a methodology called Feature Oriented Principal Components Selection (FPCS). FPCS is based on the examination of PCA eigenvector loadings to decide which of the principal component images will concentrate information directly related to the theoretical spectral signatures of specific targets. An important aspect of this approach is that it predicts whether the target surface type is highlighted by dark or bright pixels in the relevant principal component image. This methodology relies specifically on the selective input of only four image bands for PCA. (Crosta et al., 1993)

i. LANDSAT ETM+ Images

For LANDSAT TM, the bands for mapping iron oxides and clay-bearing mineral are: (TM1, TM3, TM4, and TM5) and (TM1, TM4, TM5, and TM7), respectively. It is possible to use only one band from the short-wave infrared (TM5 or TM7) in case of iron oxides, whereas only one visible band (TM1, TM2, and TM3) can be selected in case of clay-bearing minerals. (Crosta et al., 1993)

ii. ASTER data Images

The procedure for analyzing the principal components for ASTER are the same for the LANDSAT ETM+ with the exception of the greater availability of spectral information in the shortwave infrared (SWIR) region of the electromagnetic spectrum in case of ASTER due to the

increase in its SWIR bands in comparison to those of LANDSAT ETM+. This advantage enables ASTER to characterize surface materials in detail. PCA was also applied to ASTER bands that enhance iron alteration (bands 1, 3, 4, and 7), hydroxide alteration (bands 1, 4, 6 and 7). In addition Standard PCA transformation was also generated from the 9 bands (VNIR+SWIR) and the 5 bands (TIR) ASTER data respectively. (Crosta et al., 1993)

CHAPTER FOUR

RESULTS

4.1. General

The results, which have been derived from digital image processing of remotely sensed datasets of the study area, are presented and discussed in this chapter with the aim of extracting lithological, and hydrothermal alteration information that is associated with iron ore occurrences in the area of investigation. Interpretation of these images was carried out visually to identify the individual lithologies and alteration zones. Several types of image processing have been employed in this research, which are each described below in their respective subsections. Hydrothermal alteration is the one that generates mineralogical, textural and chemical changes in rocks due to the presence of hydrothermal fluids. As a result of this, new minerals are formed, which are stable in these new conditions. A few factors control this type of alterations like difference of temperature between the rock and the fluid, pH, pressure, permeability and rock composition among others.

Alteration zones are mostly broader than the targeted ore body, and so are useful in determining deposit locations. The main alteration minerals which are related to iron ore deposit are comprised of, carbonate, chlorite, limonite, sericite, haematite, jarositic, clay and among others

4.2 Color composite images

The best combinations of single spectral bands for lithologic discrimination were determined for both LANDSAT and ASTER datasets using any three band combination with low correlation coefficient between bands (Chavez et al., 1982). In general, the combination with low correlation coefficient between bands will contain most of the image information with the least amount of duplication (redundancy).The assignment of the colors (RGB) is the analyst discretion based on image enhancement favorable for geologic mapping of a specific area of investigation.

The most informative band combination should include one visible (1, 2, and 3), one NIR (4), and one SWIR (5 and 7). Based on this concept of electromagnetic spectrum regions, the best selected band combinations are: 1-4-5, 1-4-7, 3-4-5, 3-4-7, 2-4-5, and 2-4-7.

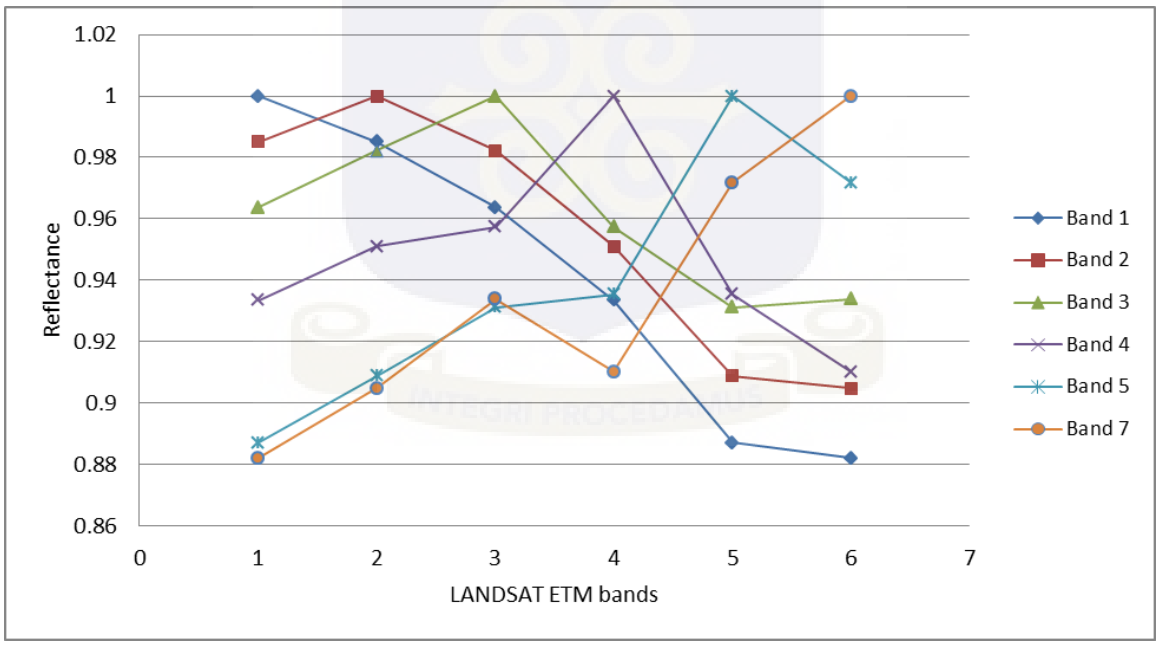

Figure 8: Correlation between LANDSAT ETM bands, Sheini Hills

Band correlation shown in Figure 8 indicates that bands 1 and 7 are uncorrelated with the rest of the other LANDSAT ETM bands; hence, any combination that includes these bands will have less redundancy, and so contains most spectral information about the mapped surfaces.

For the ASTER dataset, similar procedures have been applied to its 9 bands (VNIR and SWIR) with the aim of reducing redundancy. Comparing bands matrix plots in figure 9 it is obvious that the VNIR bands (1, and 2) with exception of band 3 which shows less redundancy as well as the SWIR bands (4, 5, 6, 7, 8, and 9). Consequently, band 3 constitutes the best band combination for mapping target surface types.

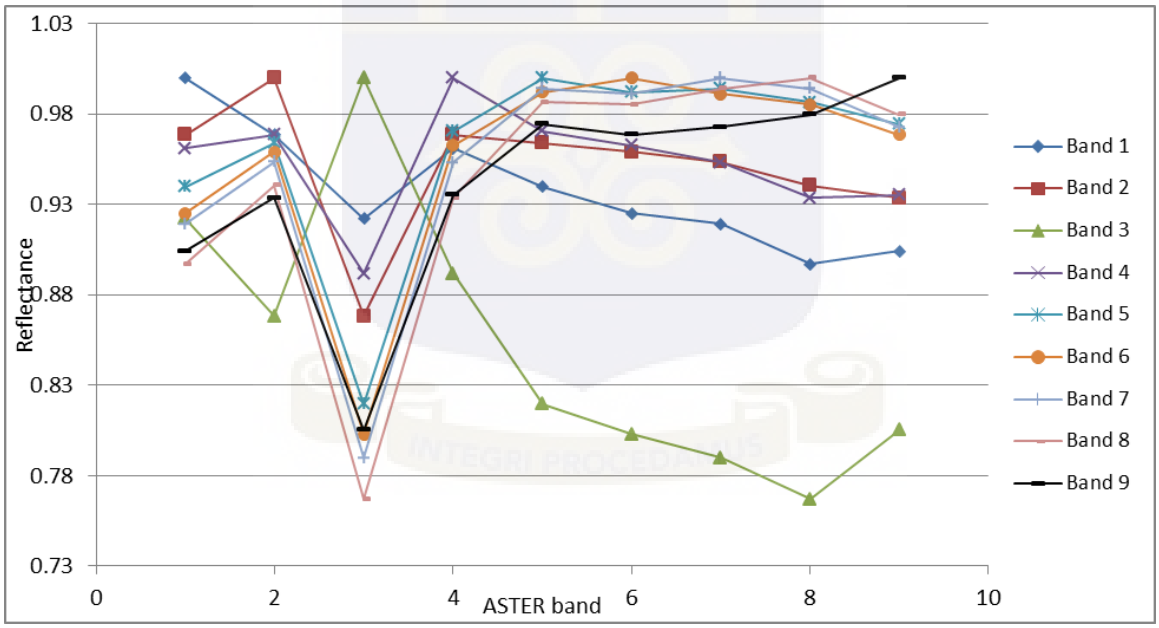

Figure 9: Correlation between ASTER bands, Sheini Hills

4.3 Principal component analysis (PCA)

In this study, the Crosta technique (Crosta et al., 1993) has been applied for PCA, whose important aspect is the prediction of whether the target surface type will be highlighted by dark or bright pixels in the relevant PC image. After application of PCA to both LANDSAT ETM and ASTER datasets of the study area, the next step was the examination of eigenvector matrix that was used in calculating these PCA with the aim of identifying which PC contains useful spectral information of the target. The more spectrally unique pixels on the ground will be highlighted by the higher numbered PC's.

Standard PCA transformation has been applied to the full ASTER scenes of the Sheini area. A total of 9 and 5 new image components were generated from the original 9 bands (VNIR + SWIR) and 5 bands (TIR) ASTER data, respectively. PCA outputs are presented as tables of statistics factors and selected PC images from these transformations are reproduced in figures to support the discussion. The image eigen vectors obtained from the PCA, using covariance matrix on all nine (VNIR+SWIR) and five (TIR) reflective bands of ASTER of the Sheini area are shown in Tables 2, and 3, respectively. Hereafter, these components are referred to Principal Component 1(PC1), PC2, through PC9 and the individual bands used for the transformation are also referred to Band 1(B1), B2, through B9

Table 2: PCA using 9 bands (VNIR + SWIR)

	B1	B2	B3	B4	B5	B6	B7	B8	B9	Percentage%
MEAN	82.6	62.7	62.4	69.8	60.6	65	60.3	58	50.3	
PC1	0.3762	0.3272	0.2687	0.353	0.3304	0.3653	0.3431	0.3417	0.2785	94.3363
PC2	0.3973	0.0973	0.6913	0.1447	-0.1709	-0.2438	-0.2793	-0.3613	-0.1915	3.8489
PC3	-0.4313	-0.4802	0.5677	-0.0828	-0.0055	-0.0282	0.0315	0.2034	0.4594	0.7146
PC4	-0.4273	-0.1591	0.0005	0.7647	0.0884	0.2255	-0.0172	-0.2179	-0.3177	0.4487
PC5	0.5072	-0.7744	-0.0979	-0.025	0.2267	0.0964	0.1749	-0.051	-0.1976	0.2603
PC6	0.1966	-0.0903	-0.3323	0.3821	0.0443	-0.3018	-0.2964	-0.2382	0.6776	0.2063
PC7	-0.0577	0.0259	0.0007	0.2009	0.1777	-0.8075	0.3918	0.2854	-0.1923	0.1156
PC8	0.1811	-0.1377	-0.0859	0.2751	-0.7276	0.0402	-0.1309	0.5595	-0.0632	0.0408
PC9	0.0055	0.0109	-0.0138	0.0139	-0.4893	0.0372	0.7169	-0.4583	0.1863	0.0286

PC1 is composed of a positive weighting of all nine (VNIR + SWIR) total bands. As indicated by the eigenvalues, PC1 accounts for 94.3363% of the total variance. Overall scene brightness, or albedo, is responsible for the strong correlation between multispectral image bands (Loughlin, 1991). PCA has effectively mapped albedo into PC1 of the transformation.PC2 to PC9 is expected to contain alteration information due to the varying spectral response of iron oxides and hydroxyl-bearing minerals (Loughlin, 1991). According to spectral characteristics, band 4 covers the spectral region (1.6 μm) where all OH-bearing minerals have maximum reflectance Fe,Mg(OH)-bearing minerals such as chlorite, as well as carbonates such as calcite and dolomite are well covered in bands 7, 8 and 9 (2.29-2.43 μm) of ASTER data (Hunt and Ashley, 1979; Mars and Rowan, 2006). By looking for moderate or large eigen vector loadings for bands 4, 7, 8

and 9 in PCs where these loadings are also in opposite sign, it can be predicted that this zones will be distinguished by bright pixels in PC4 of Tables 2 because of the positive contribution from band 4 (0.7647); while negative contributions for band 7, 8 and 9 (-0.0172,0.2179 and-0.3177). The broad phyllic zone is characterized by illite/muscovite (sericite) that indicates an intense Al-OH absorption feature centered at 2.20 □m, coinciding with ASTER band 6. Al-OH can be mapped as bright pixels in PC6 because of the positive contribution from band 4 (0.3821); while negative contributions from band 2 and 6 (-0.3018).

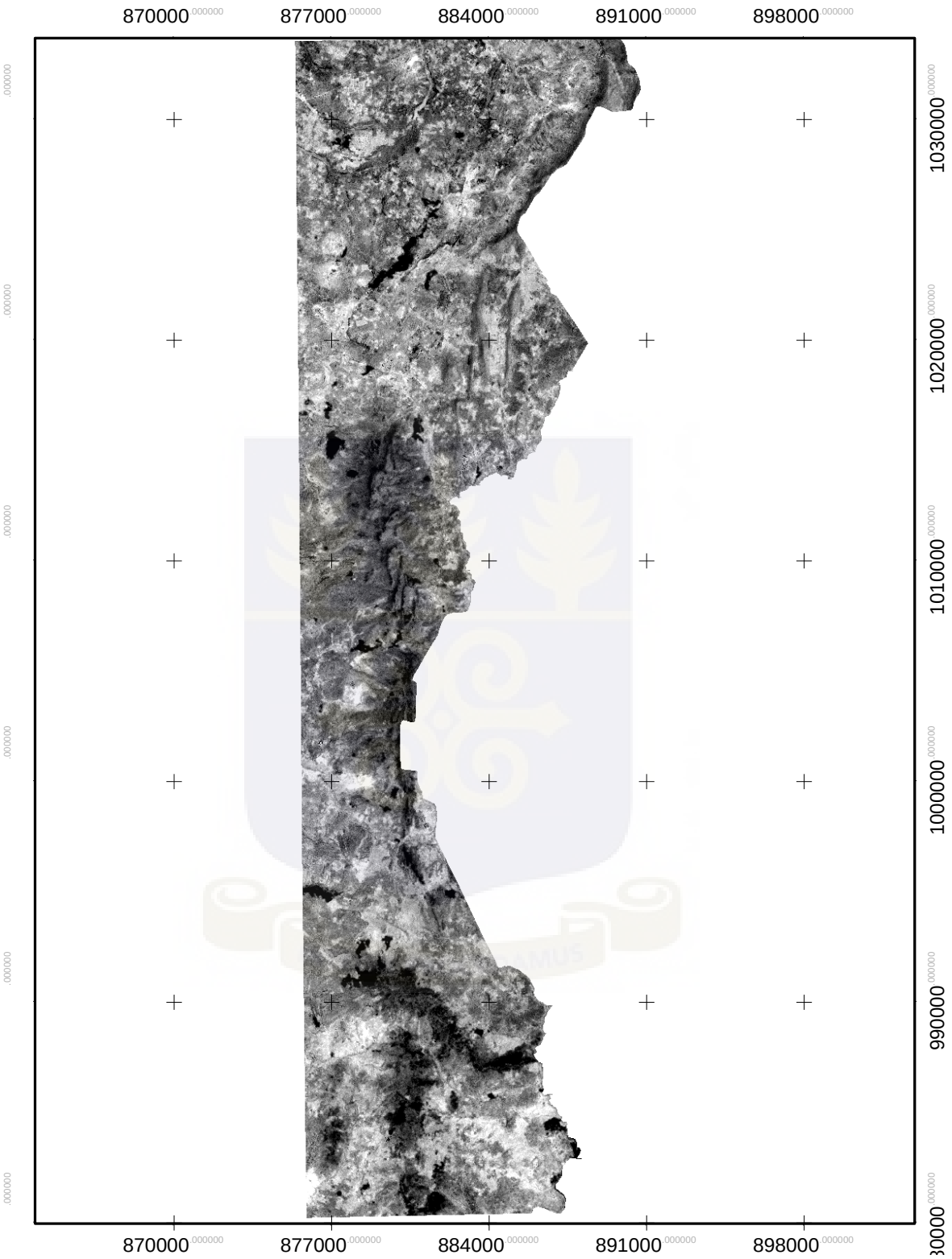

Figure 10: ASTER image (PC4) displaying Fe,Mg(OH) mineral dominant zones as bright pixels .

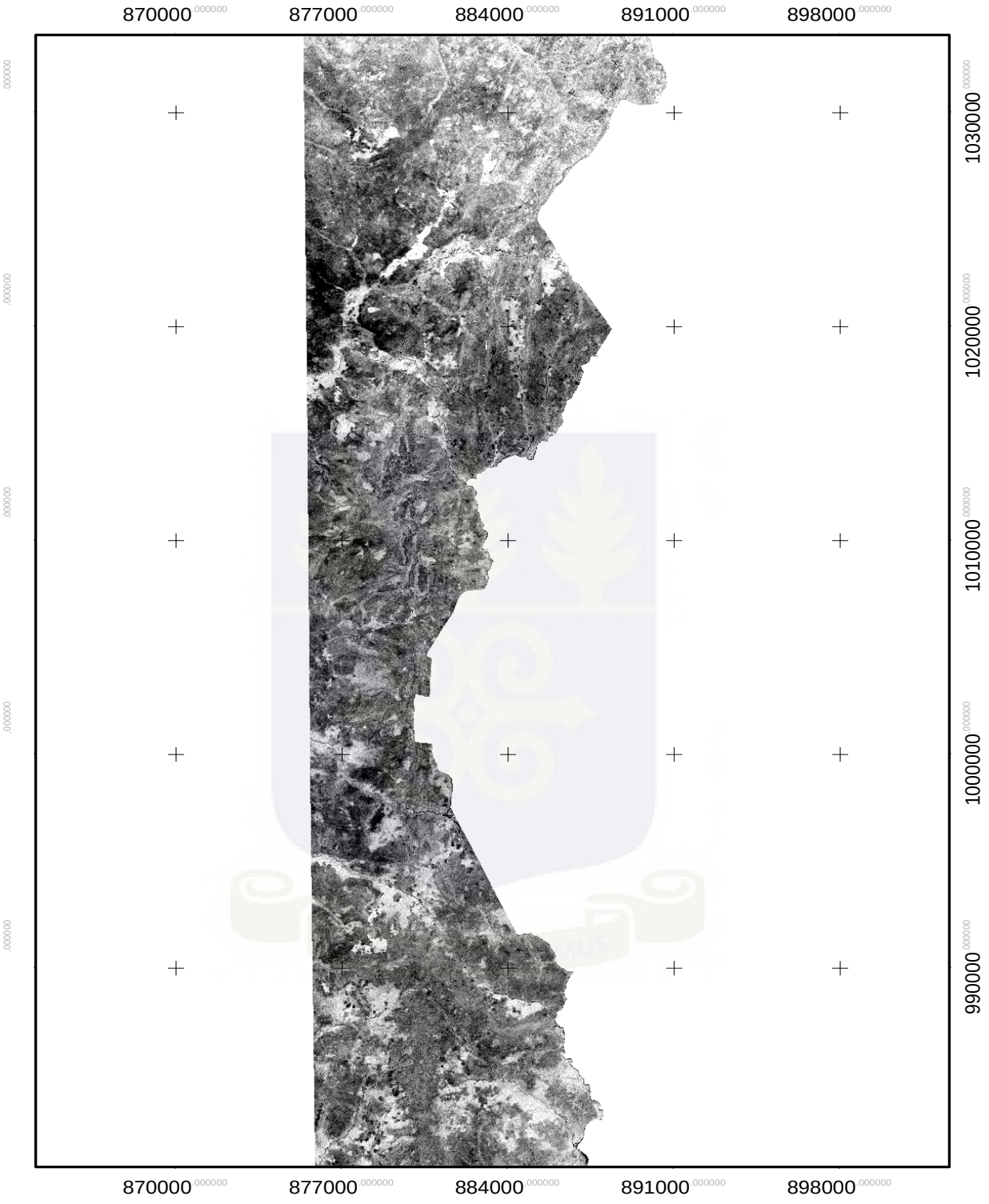

Figure 11: ASTER image (PC6) displaying AL-OH mineral dominant zones as bright pixels.

Principal components transformation was performed on original 5 band (TIR) subsystem. The TIR bands (10–14) are useful for detecting silicate and carbonate rocks (Yamaguchi et al., 1998; Ninomiya, 2003b). These bands are located in the 8.125-11.65 wavelength region and measure emitted radiation from surface materials (Yamaguchi et al., 1999).

Table 3: PCA using 5 bands (TIR)

	B10	B11	B12	B13	B14
P1	0.4406	0.4395	0.4307	0.4592	0.4651
P2	0.2366	0.3787	0.4958	-0.465	-0.5819
P3	0.8358	-0.3818	-0.2643	-0.279	0.0892
P4	-0.0655	-0.7177	0.6797	0.1349	-0.0223
P5	-0.2168	0.0514	0.1921	-0.6905	0.6608

Quartz is one of the important rock forming minerals that does not have diagnostic spectral absorption feature in the 9 VNIR+SWIR bands, but displays fundamental molecular absorption features in the TIR wavelength region. Quartz shows absorption features in bands 10 and 12 and high emissivity in bands 14 (Ninomiya, 2003b). PC1 is composed of a positive weighting of all five (TIR) total bands. As indicated by the eigenvalues. Overall scene brightness, or albedo, is responsible for the strong correlation between multispectral image bands (Loughlin, 1991). Considering the eigen vectors loadings in PC2 for recognizing quartz rich rocks in specific bands in the study area, it is evident that quartz rich rocks manifest as dark pixels because of the positive contribution from bands 10 (0.2366) and 12 (0.4958); while negative contribution from

band 14 (-0.5819). The image was then inverted in-order to display quartzite as bright pixels.

The common carbonate minerals, calcite and dolomite, have an absorption feature at band 14 and high emissivity at band 13 (Ninomiya, 2003b; Rockwell and Hofstra, 2008). It is evident carbonate minerals manifest as dark pixels on PC3 because of the negative contribution from band 13 (-0279) while positive contribution from bands 14 (0.0892).

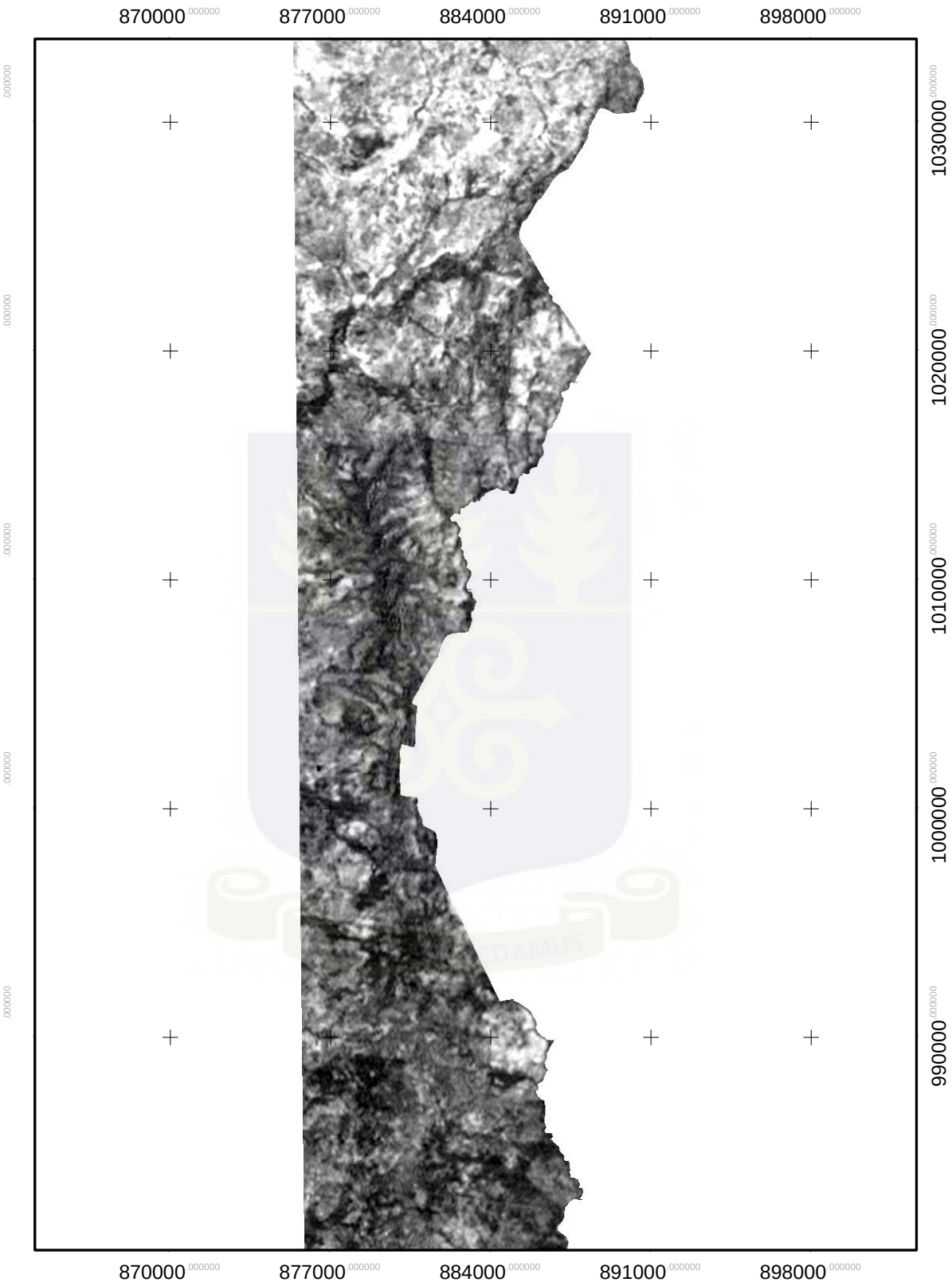

Figure 12: ASTER PC2 showing quartz rich rock as bright pixels.

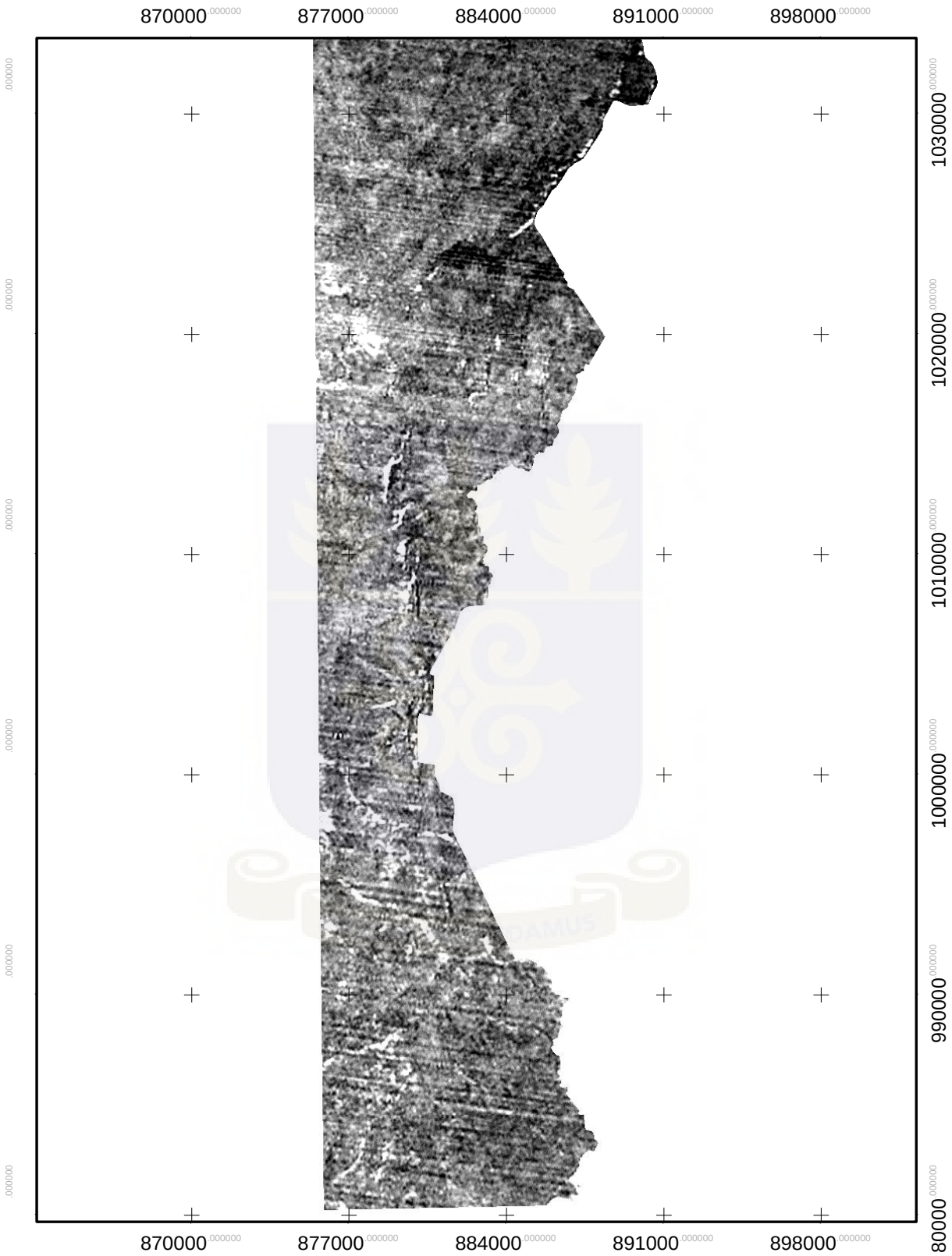

Figure 13: PC 3 showing carbonate mineral dominant zones as bright pixels.

4.3.1 Feature-oriented principal component selection (FPCS)

This method accounts only for the bands that exhibit spectral signatures caused by Fe and OH bearing minerals. PC transformation was applied to both LANDSAT ETM and ASTER images of the study area whose statistical analysis, eigenvalues, and eigenvector loadings are tabulated below. For LANDSAT ETM, the bands for mapping iron oxides and clay-bearing mineral are: (ETM1, ETM3, ETM4, and ETM5) and (ETM1, ETM4, ETM5, and ETM7), respectively. It is possible to use only one band from the short-wave infrared (TM5 or TM7) in case of iron oxides, whereas only one visible band (TM1, TM2, and TM3) can be selected in case of clay-bearing minerals. FPCS for iron oxides and clay minerals have been determined as shown in Tables 4 and 5, respectively.

Table 4: FPCS for iron oxide minerals using LANDSAT TM bands (1, 3, 4, and 7).

	B1	B3	B4	B7
P1	0.58586	-0.02753	0.59642	-0.54799
P2	-0.47424	-0.22315	0.77664	0.34948
P3	0.45806	-0.78694	-0.12389	0.39441
P4	0.47122	0.57461	0.16052	0.64962

As illustrated (Table 4) by the loadings of bands TM1 and TM3 on PC3, which are positive (reflectance) and negative (absorption) respectively, anomalous iron-oxides minerals will be

represented by dark pixels in PC3, therefore PC3 was inverted to display anomalous iron oxide minerals as bright pixels

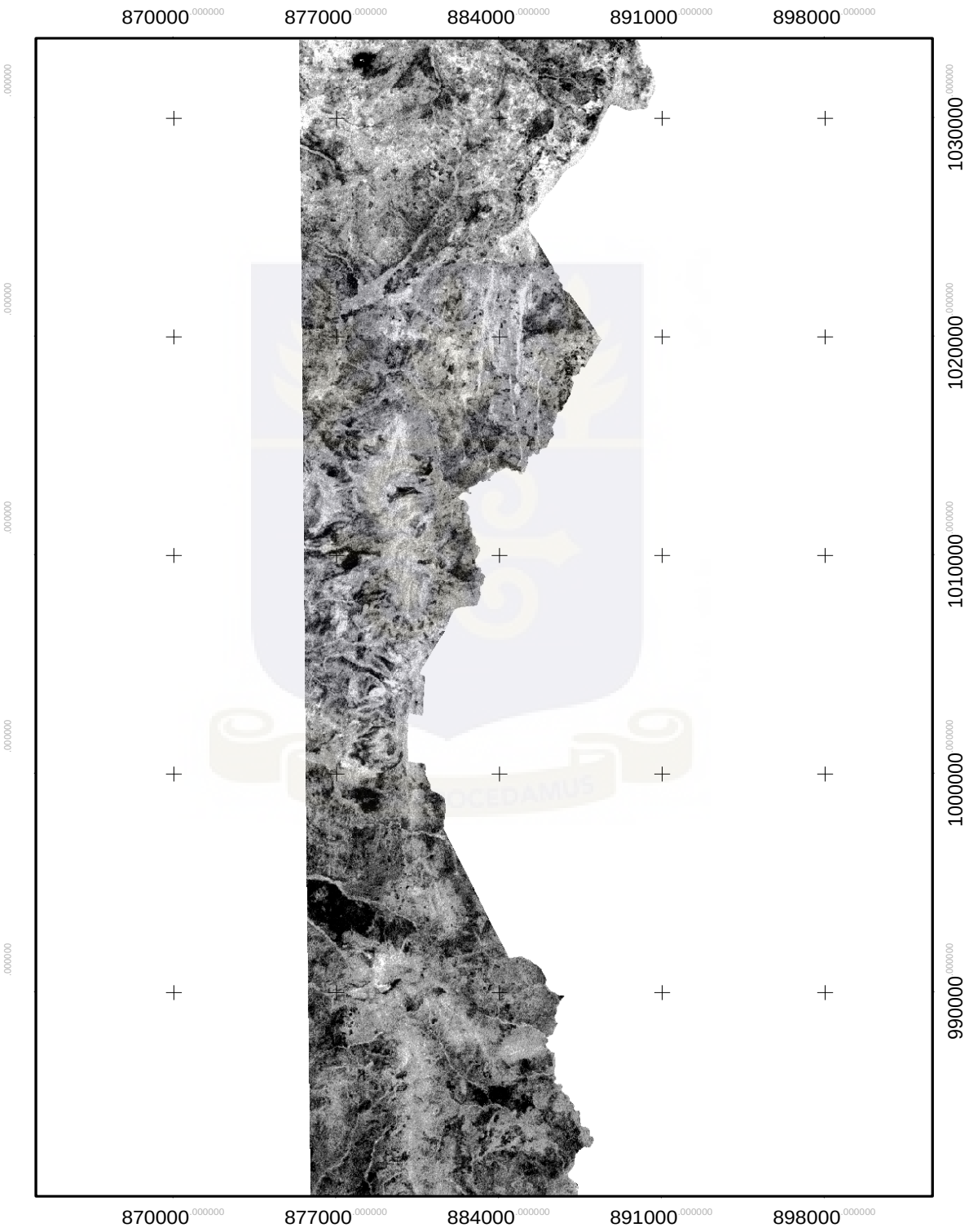

Figure 14: LANDSAT ETM (PC3) image showing FPCS for Iron oxides mineral dominant zones as bright pixels. There is a better correspondence between the Landsat derived Iron anomalies and mapped iron formations/ferricretes.

Table 5: FPCS for clay minerals using LANDSAT TM bands (1, 4, 5, and 7).

	B1	B4	B5	B7
P1	0.58211	0.59416	-0.1296	-0.55494
P2	-0.64016	0.45352	0.58708	-0.19964
P3	-0.19476	0.64659	-0.54163	0.50063
P4	0.46196	0.15238	0.60151	0.63368

Hydroxyl-bearing minerals will be highlighted as bright pixels in PC2 because of the magnitudes and eigenvector loadings of ETM5 and ETM7 are positive (0.58708) and negative (-0.19964) respectively.

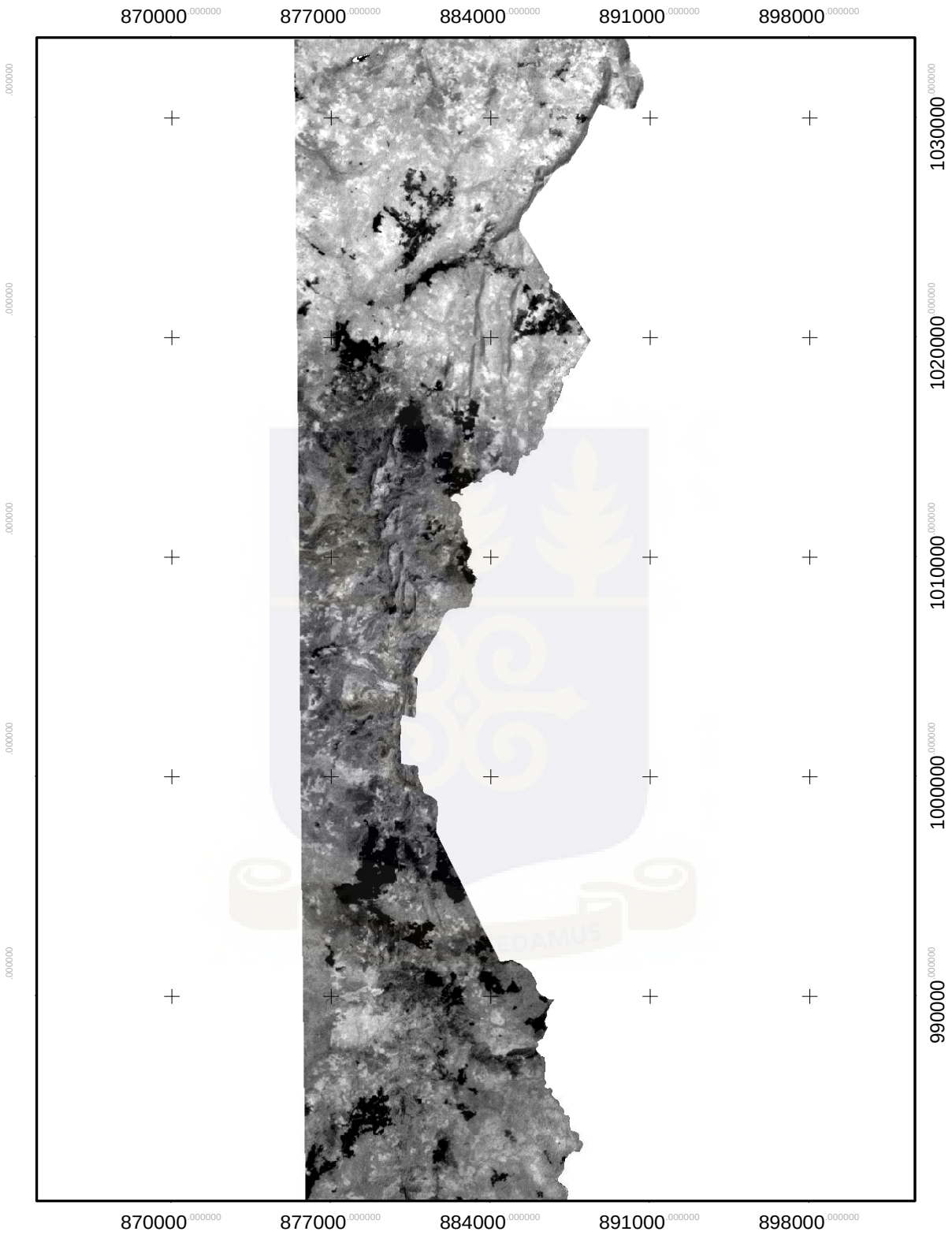

Figure 15: LANDSAT ETM (PC2) image showing FPCS for Iron Hydroxyl mineral dominant zones as bright pixels.

The procedure for analyzing the principal components for both LANDSAT and ASTER are the same with the exception of the greater availability of spectral information in the shortwave infrared (SWIR) region of the electromagnetic spectrum in case of ASTER due to the increase in its SWIR bands in comparison to those of LANDSAT. This advantage enables ASTER to characterize surface materials in detail. PCA was also applied to ASTER bands that enhance iron alteration (bands 1, 3, 4, and 7) as shown in Table 6. It can be observed from computed statistics of the ASTER FPCs that PC4 enhances ferric oxide minerals as bright pixels because of the positive contribution of band 3(0.3804) and negative contribution of band 1(-0.1065).

Table 6: FPCS for iron oxide minerals using ASTER bands (1, 3, 4, and 7).

	B1	B3	B4	B7
P1	0.563	0.4173	0.5201	0.4883
P2	0.1582	0.7298	-0.1482	-0.6483
P3	-0.8042	0.3854	0.4306	0.1392
P4	-0.1065	0.3804	-0.7226	0.5674

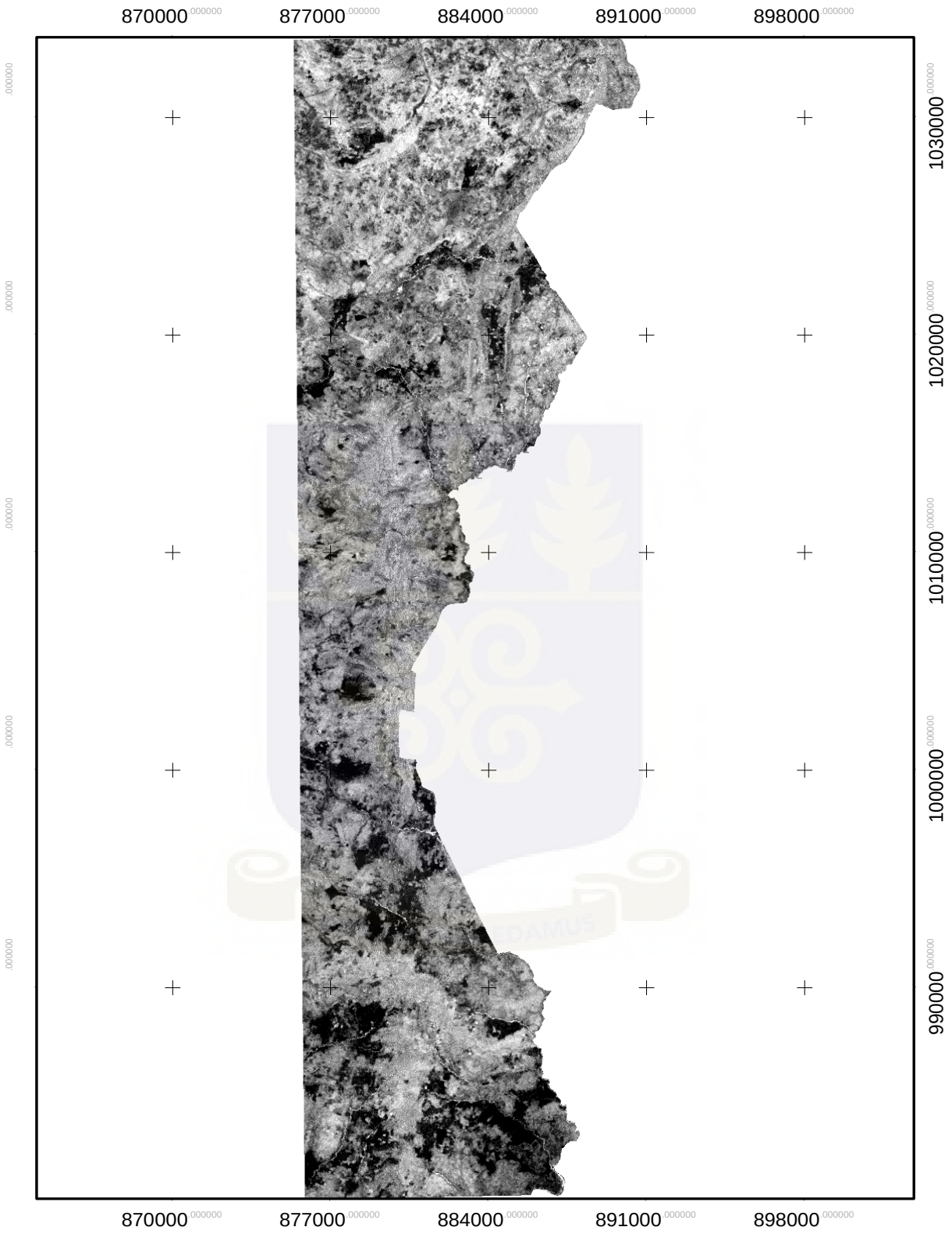

Figure 16: ASTER (PC4) image showing FPCS for ferric oxides mineral dominant zones as bright pixels.

For mapping clay minerals with FPCS method, it is appropriate to use the diagnostic features of Al-OH-bearing minerals (kaolinite, montmorillonite, and illite) in addition to buddingtonite and alunite. The major absorption by these minerals occurs within bands 5 and 6. The statistics listed in Table 7 indicates negative contribution by band 4(-0.8424) and positive contribution by 6(0.0812) on PC3, hence, PC3 enhances rocks containing Al-OH (clay) minerals. The image was then inverted to show brighter pixels as Al-OH minerals

Table 7: FPCS for clay minerals using ASTER bands (1, 4, 6, and 7).

	B1	B4	B6	B7
P1	0.5241	0.4918	0.5072	0.4755
P2	-0.7268	-0.1659	0.458	0.4842
P3	0.4418	-0.8424	0.0812	0.2977
P4	-0.043	0.1448	-0.7255	0.6715

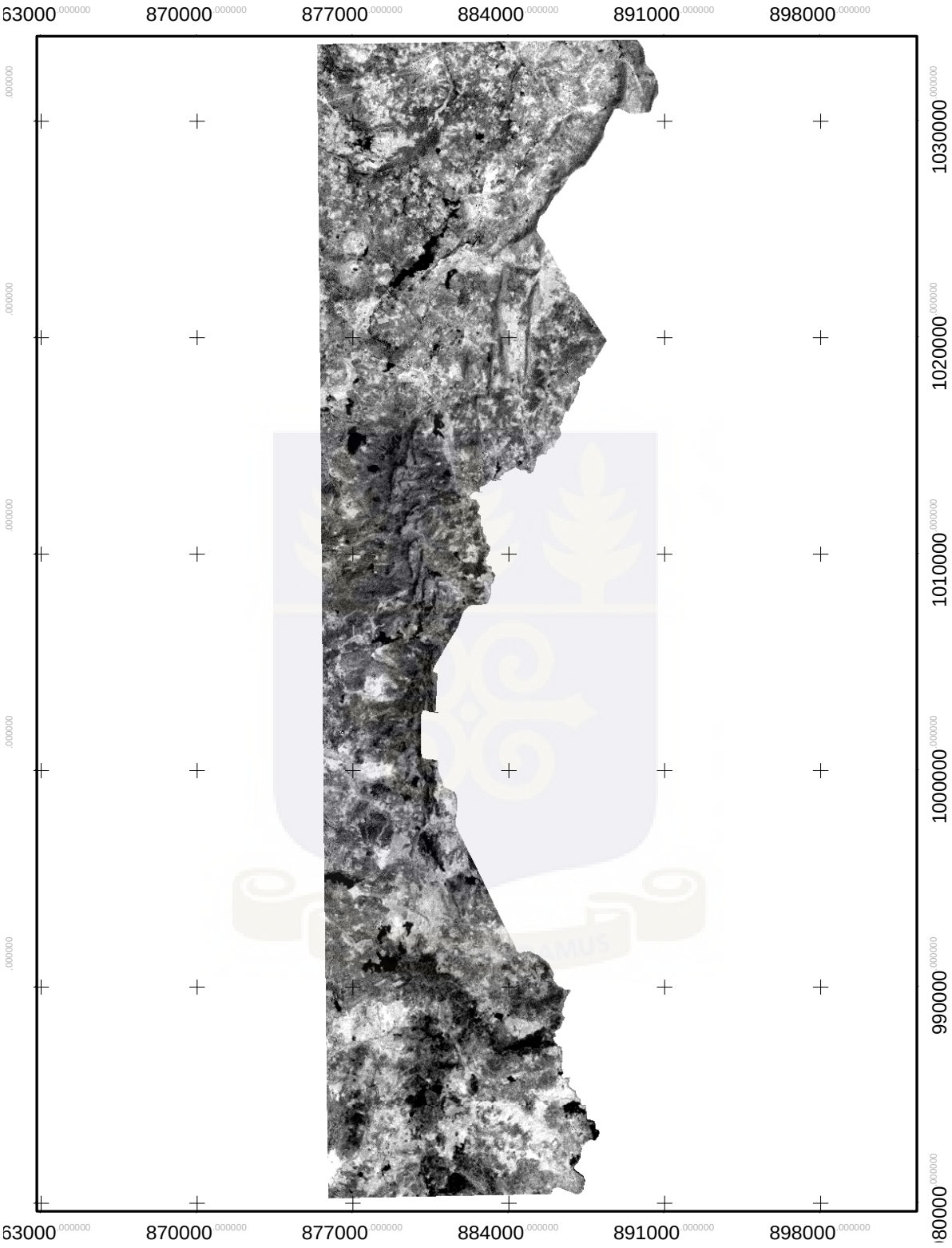

Figure 17: PC3 enhances rocks containing Al-OH (clay) mineral dominant zones as brighter pixels

4.4 .Band ratio

Groups of minerals with strong absorption bands at similar wavelengths can be detected by ratioing ETM bands to enhance the presence of these absorption bands. One group (clay-carbonate-sulfate-mica minerals) is characterized by strong absorption near 2.2-2.3 (μm), which occurs in ETM band 7, and includes hydroxyl-bearing minerals (for example, clay and mica minerals), hydrated sulfates (for example gypsum and alunite), and carbonate minerals (calcite and dolomite). The ETM 5/7 ratio is used to detect the strong absorption of the clay-carbonate-sulfate-mica group minerals in ETM band 7 (Knepper, 1989). Because of the strong absorption, the DN in ETM band 7 is low, producing high ratio values.

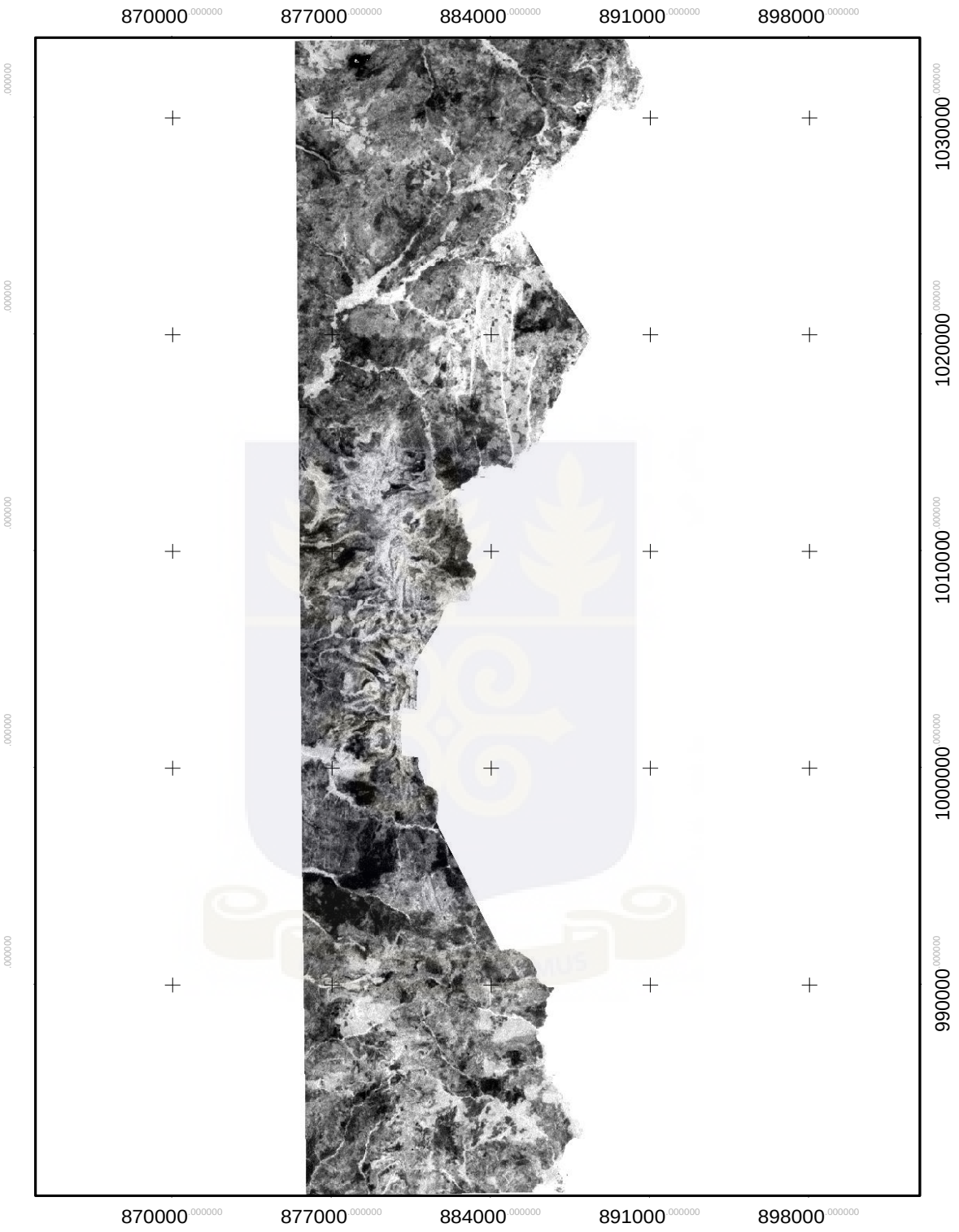

Figure 18: Landsat ETM Band ratio 5/7 showing clay-carbonate-sulfate-mica minerals areas of as bright pixels. Many of the larger carbonate anomalies coincide with broad areas of alluvium.

The second group is typified by ferric iron minerals (including hematite, goethite, and jarosite) that typically are shades of red, yellow, and orange in the visible region of the electromagnetic spectrum and have strong absorption in the ultraviolet portion of the spectrum that also strongly affects ETM bands 1 (blue) and 2 (green). The ETM 3/1 ratio is used to detect the reddish colors that ferric iron minerals give to rocks and soils. The red colors are expressed as high DN values in ETM band 3 (red band) and low DN values in ETM band 1 (blue band) because of the strong absorption in the ultraviolet and blue portion of the spectrum. Consequently, high 3/1 ratio values are indicative of the presence of minerals of the ferric iron mineral group.

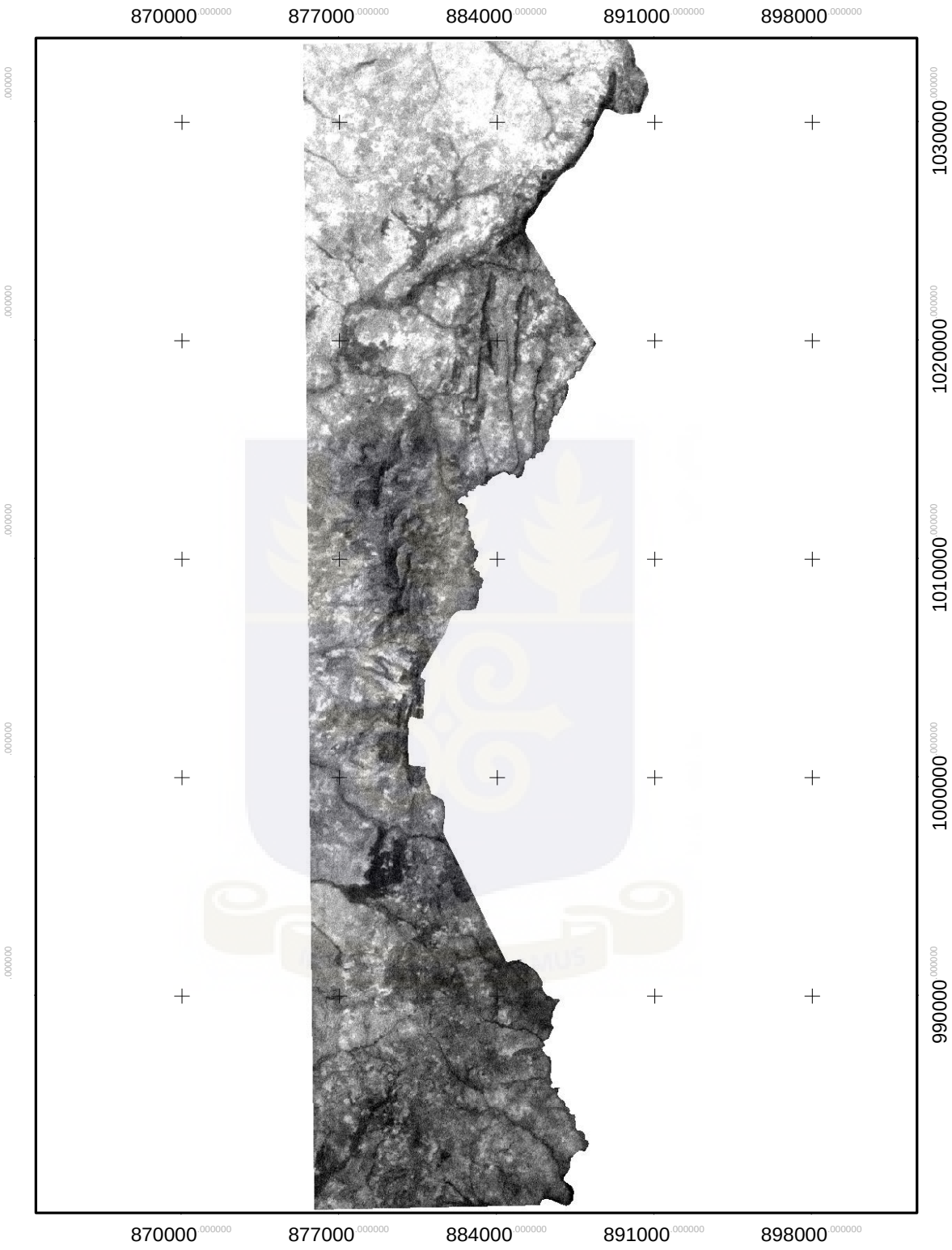

Figure 19: Landsat ETM Band ratio 3/1 showing areas of Ferric Iron Minerals (including hematite, goethite, and jarosite) in bright pixels.

A third TM band ratio, 5/4, is used in TM color-ratio composite images specifically to visually separate high 5/7 ratio values caused by vegetation from those caused by clay-carbonate-sulfate minerals. Because green vegetation is distinctively highly reflective in TM band 4, the 5/4 ratio values of vegetated areas are low compared to areas of bare rock and soil. The 5/4 ratio values are color-coded blue on the color-ratio composite image map such that areas with bare rock and soil (high 5/4 values) have a blue component. Since vegetated pixels were eliminated from the analysis using the NDVI mask, the 5/4 ratio serves only as a check that all vegetation was successfully eliminated. Notice in figure 22 that there are abundant magenta pixels (high 5/7 and 5/4 values indicating clay-carbonate-sulfate-mica group minerals) and no obvious red pixels (high 5/7 only possibly indicating green vegetation pixels) indicating that vegetation masking was effective.

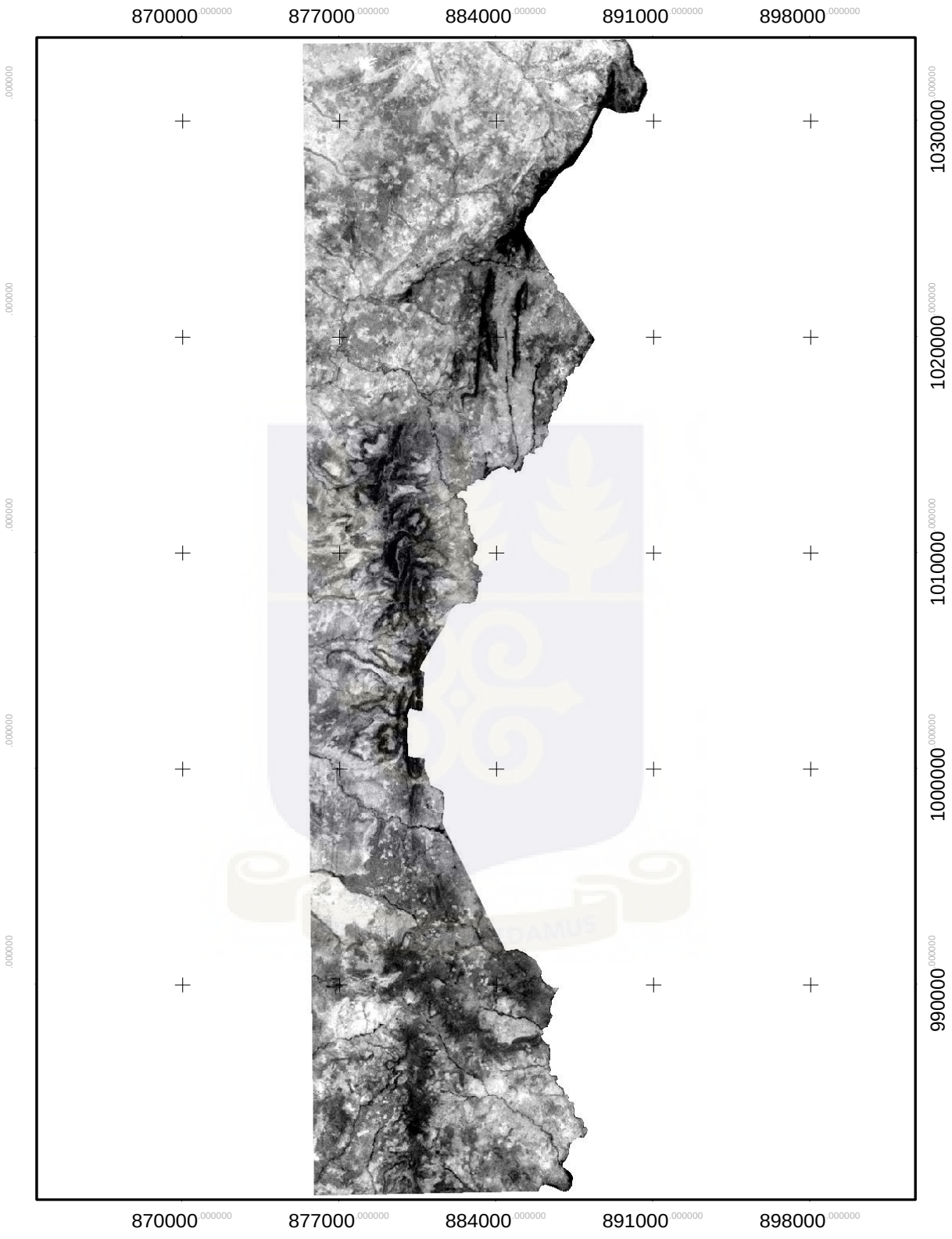

Figure 20: Landsat ETM Band ratio 5/4 showing bare grounds in bright pixels

Each non vegetated pixel in the map area has a 5/7, 3/1, and 5/4 ratio value and these values are displayed in red, green, and blue hues, respectively, proportional to their values. The higher the ratio value, the more of its color is represented in the pixel. The respective colors for the three ratio values are combined in the color-ratio composite image map by the color additive process illustrated in figure 22. High values of only one of the ratio values will be displayed in hues of its respective primary color: red (5/7), green (3/1), or blue (5/4). Two ratios with high values will be displayed as the combination of their two primary colors. For example, a pixel with a high 5/7 ratio (clay-carbonate-sulfate-mica) and a high 3/1 ratio (iron oxide) will be displayed yellow (red + green) if both ratios are of a similar value. If the 5/7 value is higher than the 3/1 value, the pixel will be orange. If the 3/1 is larger than the 5/7, the pixel will be yellowish-green,

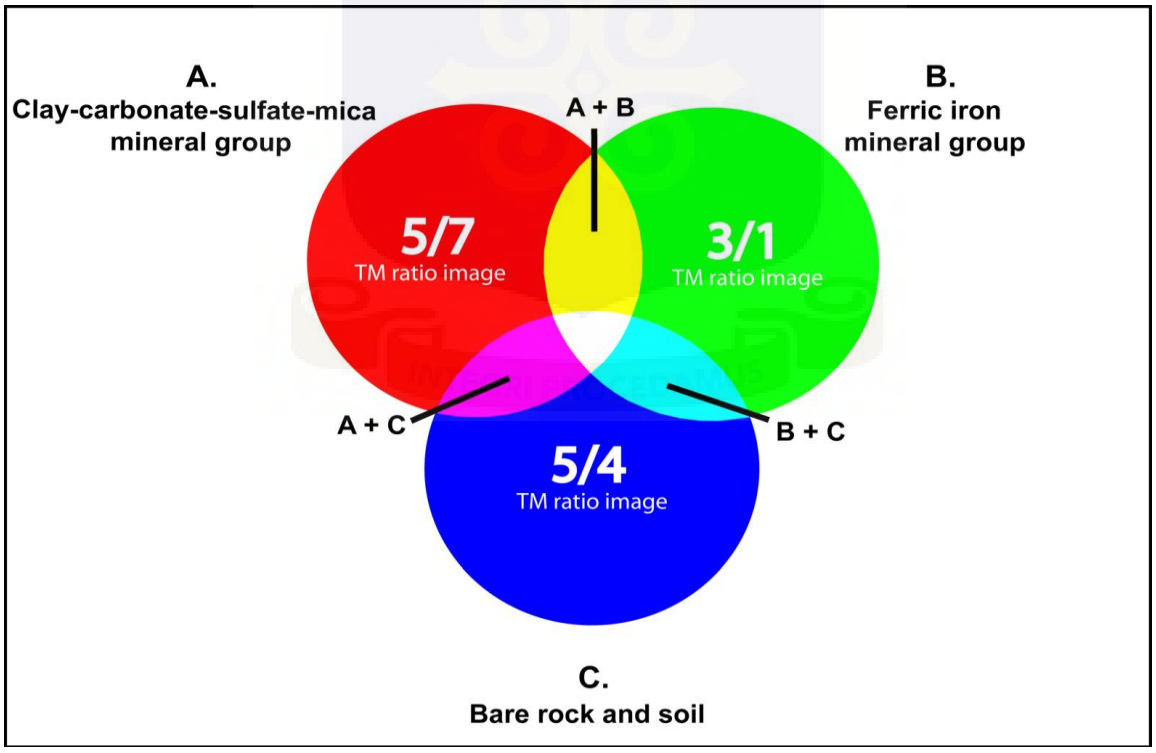

Figure 21: Generalized colors obtained by color addition of combined red, green, and blue images.

The three Landsat Thematic Mapper (TM) ratio images (5/7, 3/1, 5/4) were combined as red, green, and blue, respectively. Pixels with a high 5/7 ratio will have large red component. Large 3/1 ratio values will give a pixel a large green component. Since vegetation was filtered out prior to combining the three ratio images, the high 5/4 ratio values produced by bare ground (and some ferric and ferrous iron minerals) will give each pixel a blue component. By recognizing the basic hues produced by color addition (red, magenta, blue, cyan, green, yellow, and white), the general composition derived from the spectral information can be inferred.

The second group is typified by ferric iron minerals (including hematite, goethite, and jarosite) that typically are shades of red, yellow, and orange in the visible region of the electromagnetic spectrum and have strong absorption in the ultraviolet portion of the spectrum that also strongly affects ETM bands 1 (blue) and 2 (green). The ETM 3/1 ratio is used to detect the reddish colors that ferric iron minerals give to rocks and soils. The red colors are expressed as high DN values in ETM band 3 (red band) and low DN values in ETM band 1 (blue band) because of the strong absorption in the ultraviolet and blue portion of the spectrum. Consequently, high 3/1 ratio values are indicative of the presence of minerals of the ferric iron mineral group

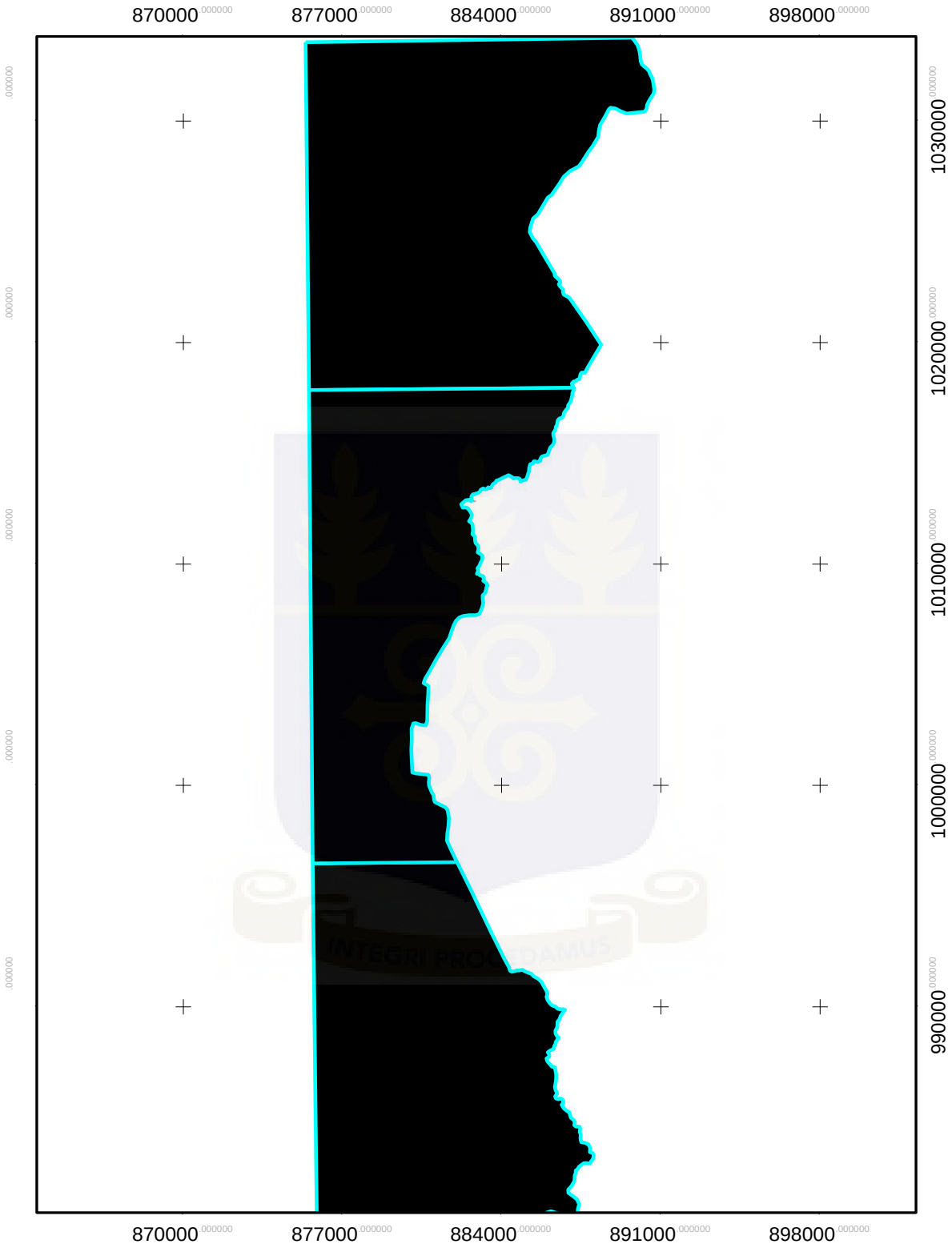

Figure 22: LANDSAT ETM image of band ratios R (5/7), G (3/1), and B (5/4) as RGB for Sheini Hills

Since green vegetation has been masked, all pixels contain a blue component from moderate to high 5/4 ratio values indicating bare rock and soil. Consequently, high 5/7 (red) also has a blue component and appears in shades of magenta (red + blue). Similarly, pixels bearing ferric iron (high 3/1 values) tend toward cyan hues (blue + green). Visually, the effect of the blue component on a pixel with both high 5/7 and 3/1 ratio is not particularly obvious, but it tends to vary the brightness and shade of yellow,

ASTER Ratio images used in this study was prepared by applying the ratio codes and spectral ratioing method introduced by Vincent (1997). The method enabled extraction of spectral information from ASTER datasets. Band ratios (4/5, 4/3, 2/1) of ASTER image (Fig.23) which is equivalent to (5/7, 3/1, 5/4) of Landsat ETM (Kalin Rouskov et al., 2005) are used for mapping of iron ores and associated lithological units.

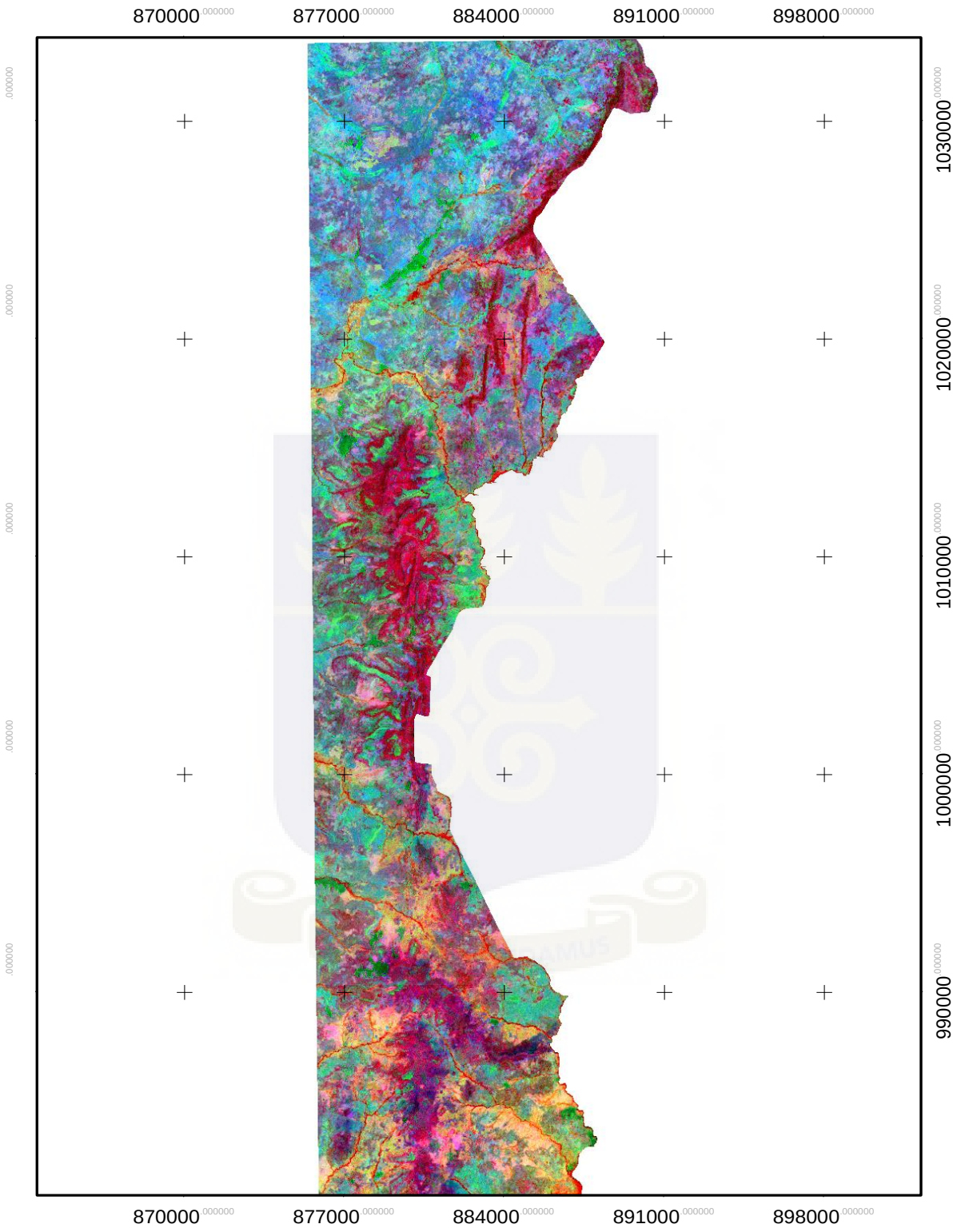

Figure 23: ASTER image of band ratios R (4/5), G (2/1) and B (4/3) as RGB for Sheini Hills

In this research, before lithologic discrimination was performed, the contributions to the area scene by vegetation cover were identified first using LANDSAT ETM band combinations 4-3-2 and ASTER bands 3-2-1 in RGB colors, which revealed vegetation as red feature.

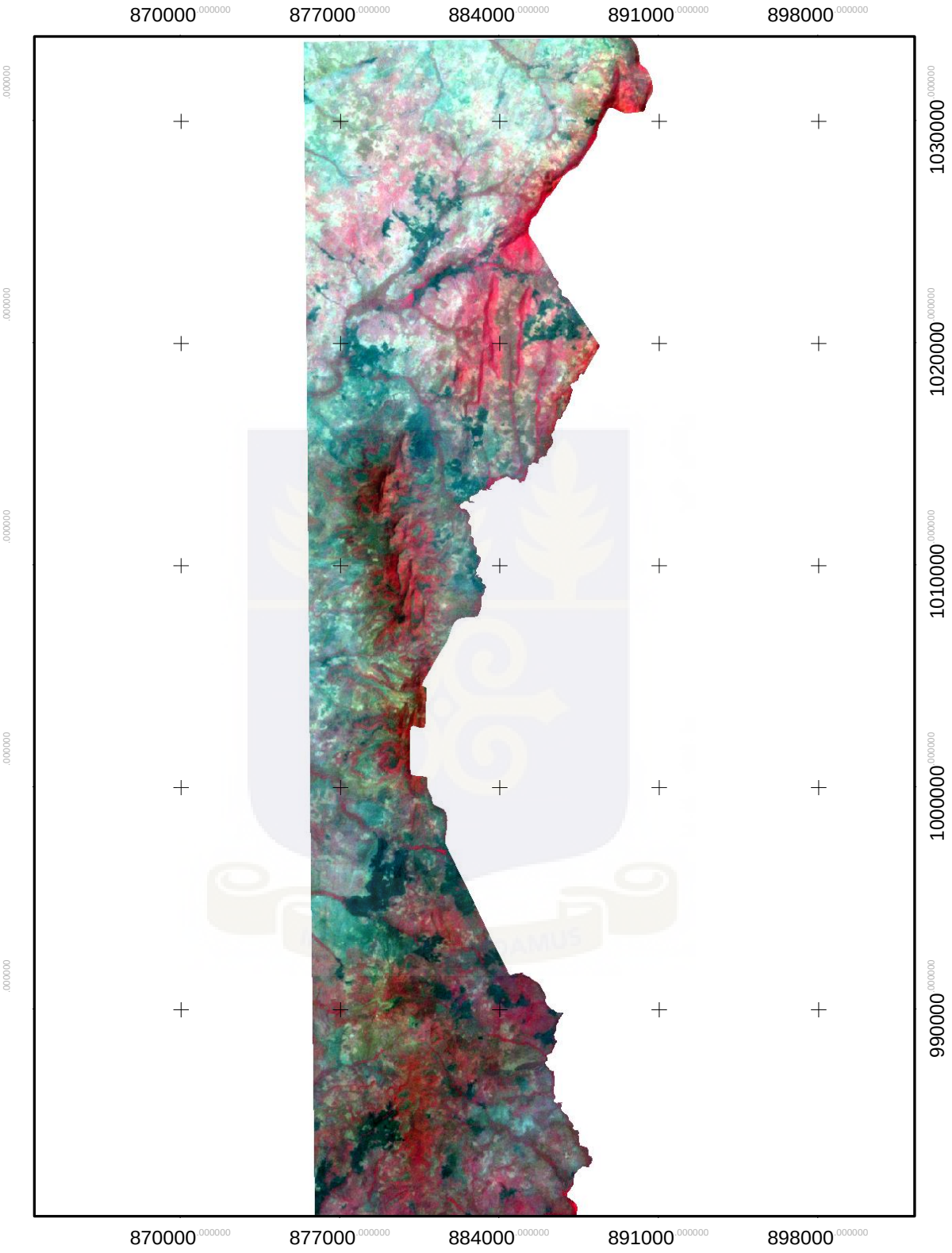

Figure 24: Vegetation cover appears red in LANDSAT TM image 4-3-2 (RGB) for Sheini Hills

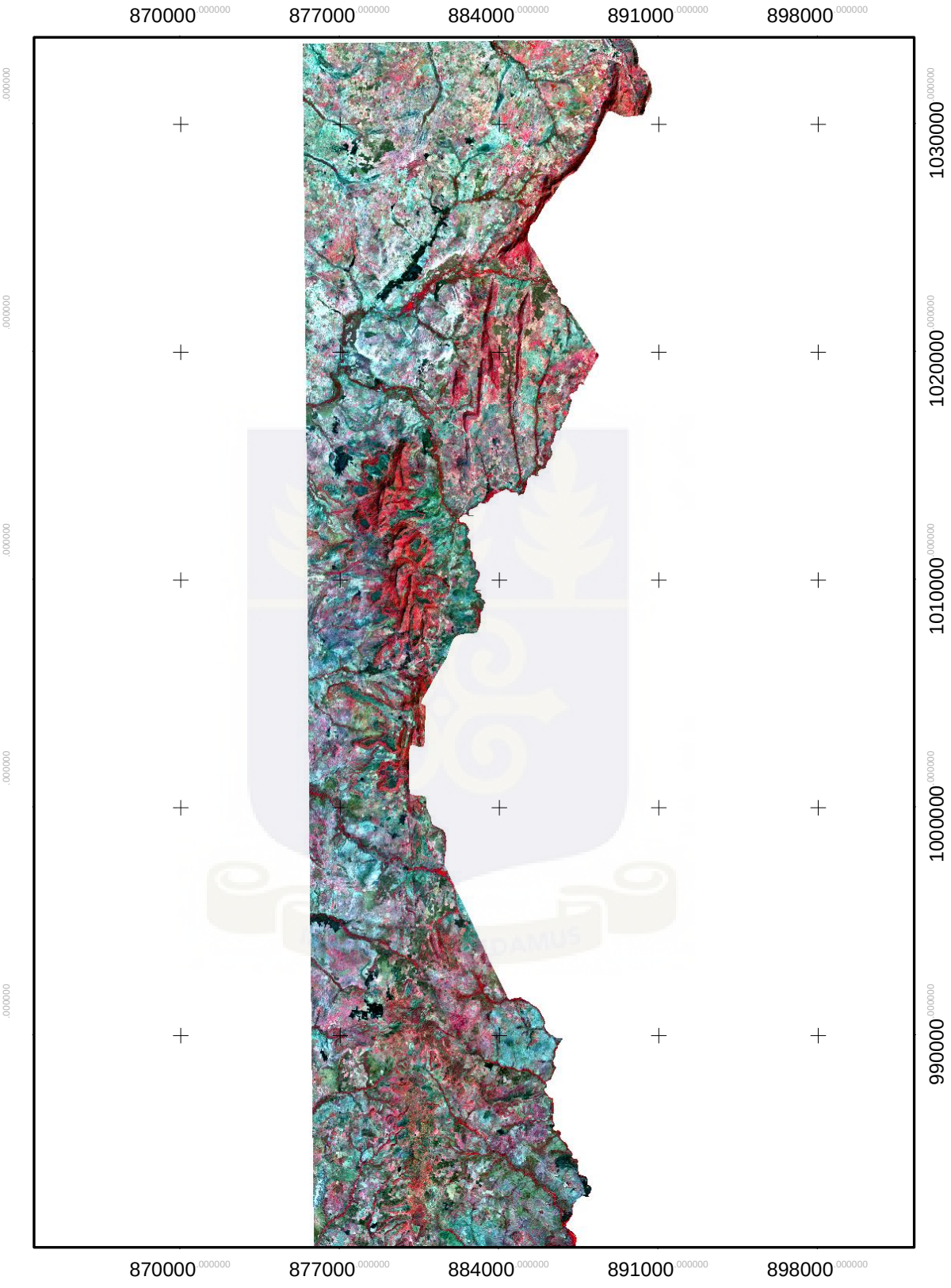

Figure 25: ASTER bands 3-2-1 (RGB) showing vegetation cover as red for Sheini Hills

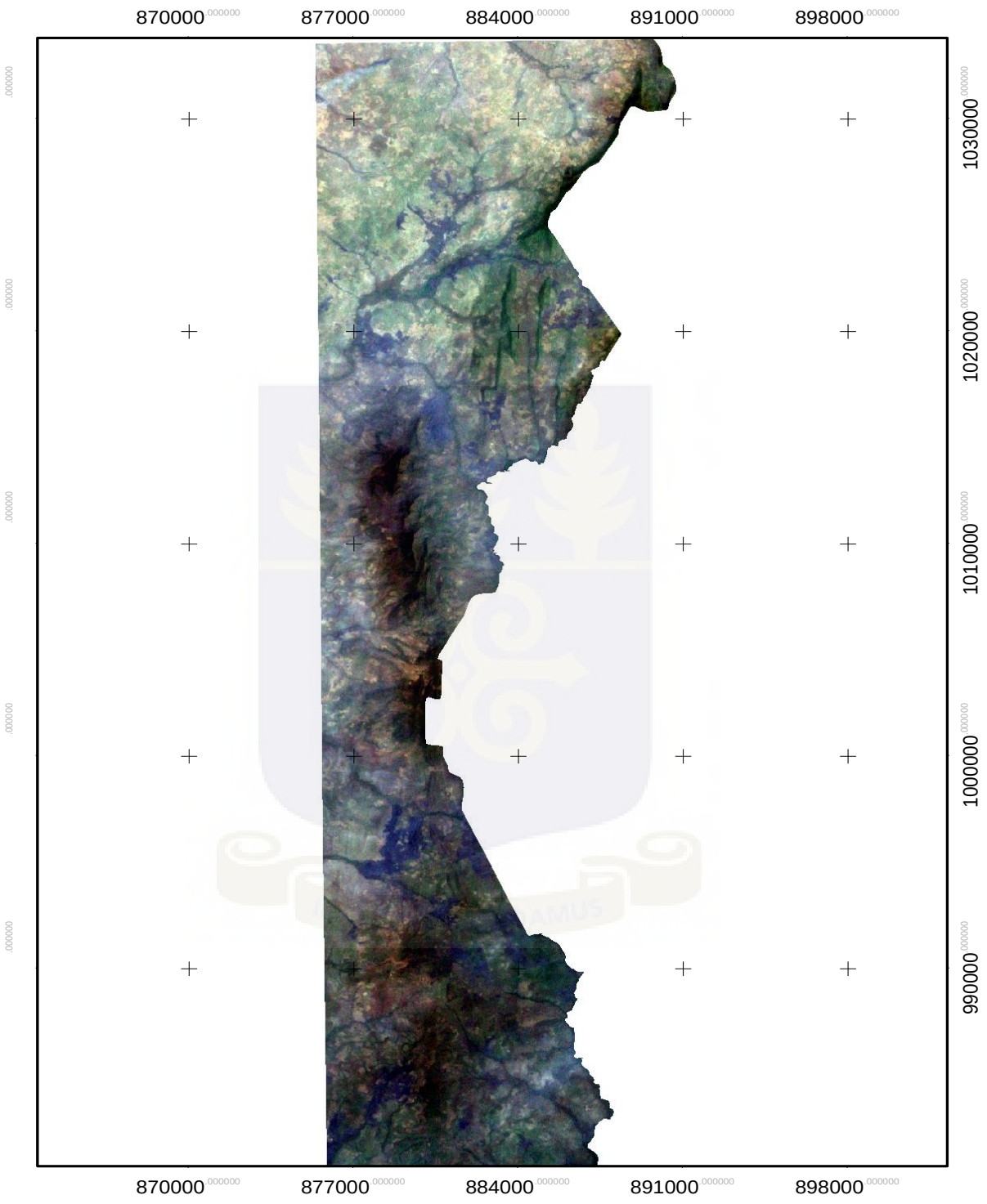

Figure 26: LANDSAT ETM bands 3-2-1 (RGB) which is a true color composite image for Sheini Hills

Examination of the true color composite image of the area displays geologic features as it would be visualized by the human eye. A better contrast in images of the study area was obtained by selecting the best three uncorrelated band combination as shown below.

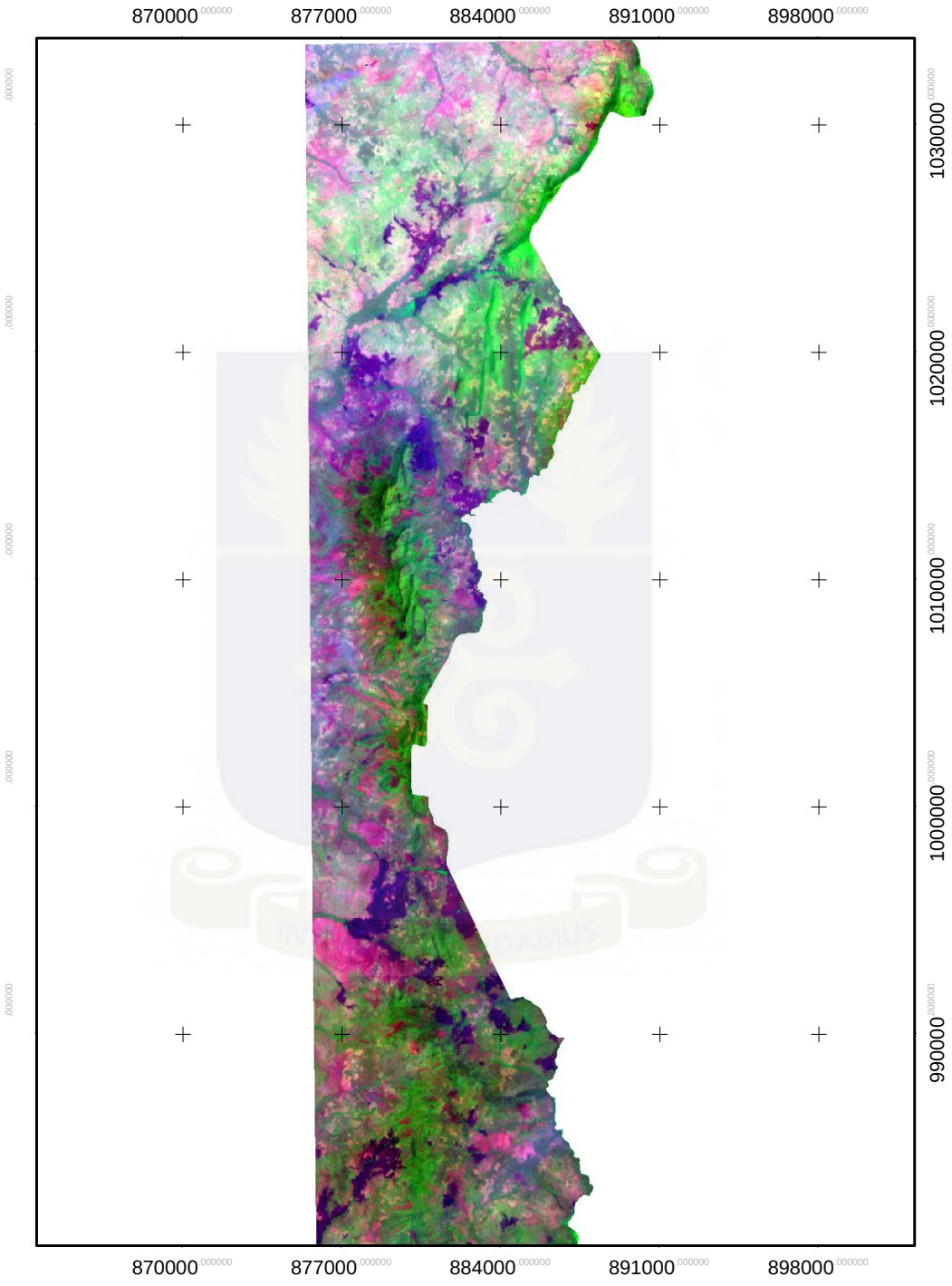

Figure 27: LANDSAT ETM 7- 4 -1 (RGB) False Color Composite FCC image of the study area.

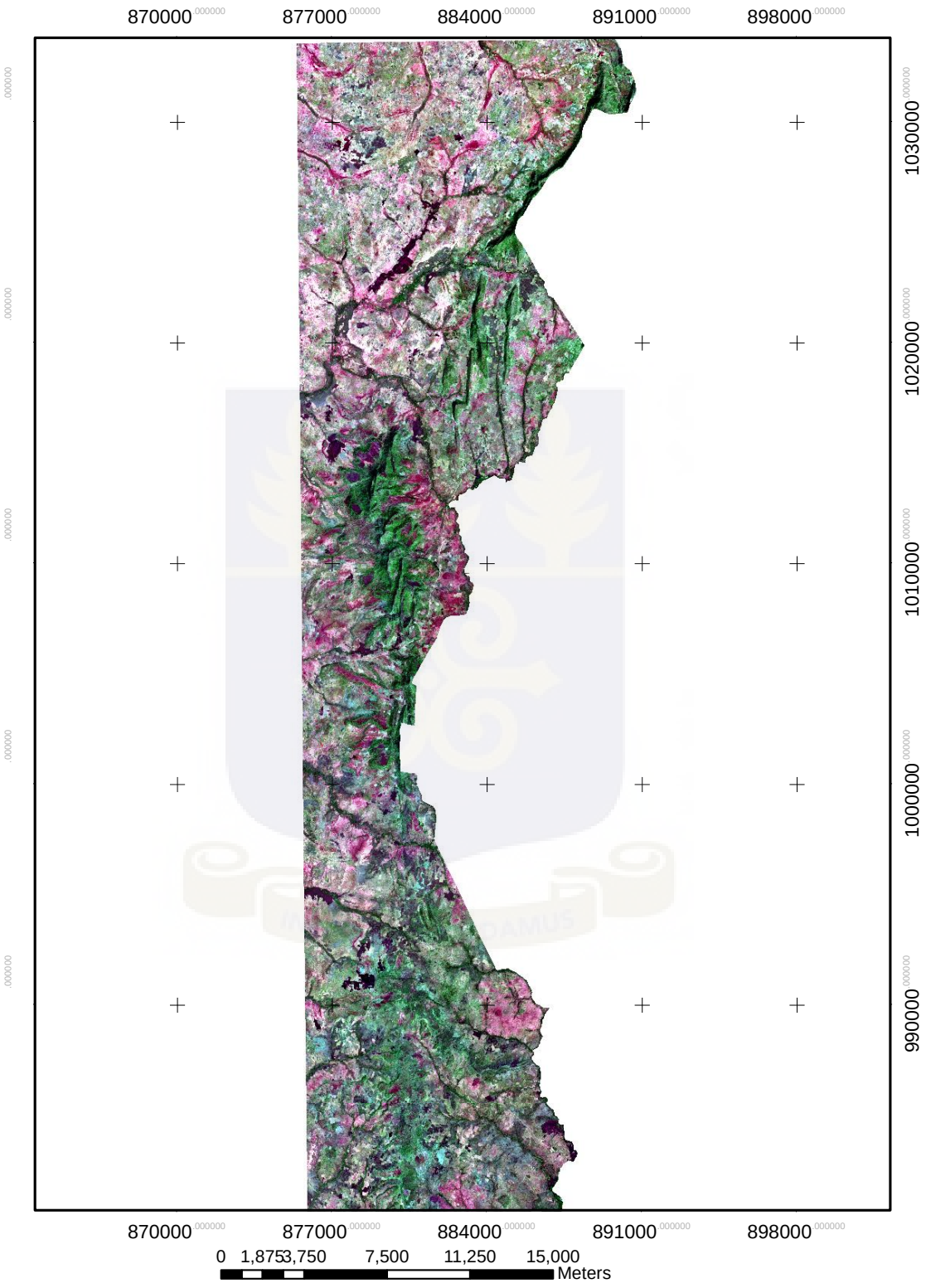

Figure 28: ASTER FCC image for bands 7-3-2 (RGB), Sheini Hills.

Discrimination of gossans(red) in this area was performed using ASTER band combination 6-2-1 (RGB), (Kalinowski et al., 2004) and ASTER band ratios R (4/1), G (3/1), and B (4/5) as illustrated in Figure 29 and 30 respectively. Iron oxides are created during supergene alteration and render characteristic yellowish or reddish color to the altered rocks that termed gossans (Abdelsalam and Stern, 2000; Xuet al., 2004)

Figure 29: ASTER band combination 6-2-1 (RGB) illustrates gossans in reddish-brown color.

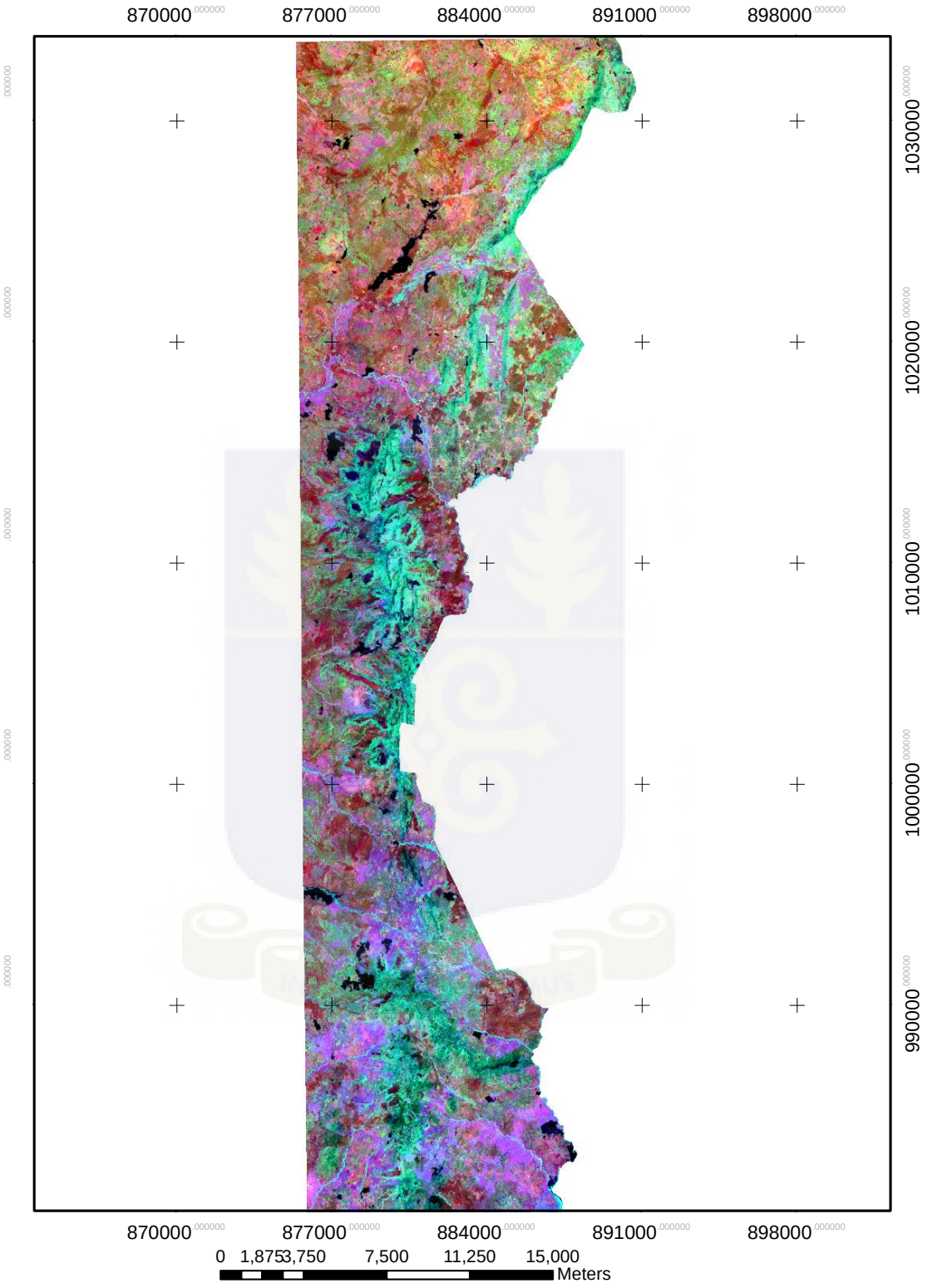

Figure 30: Gossans mapping using ASTER band ratios R (4/1), G (3/1), and B (4/5) as RGB, respectively.

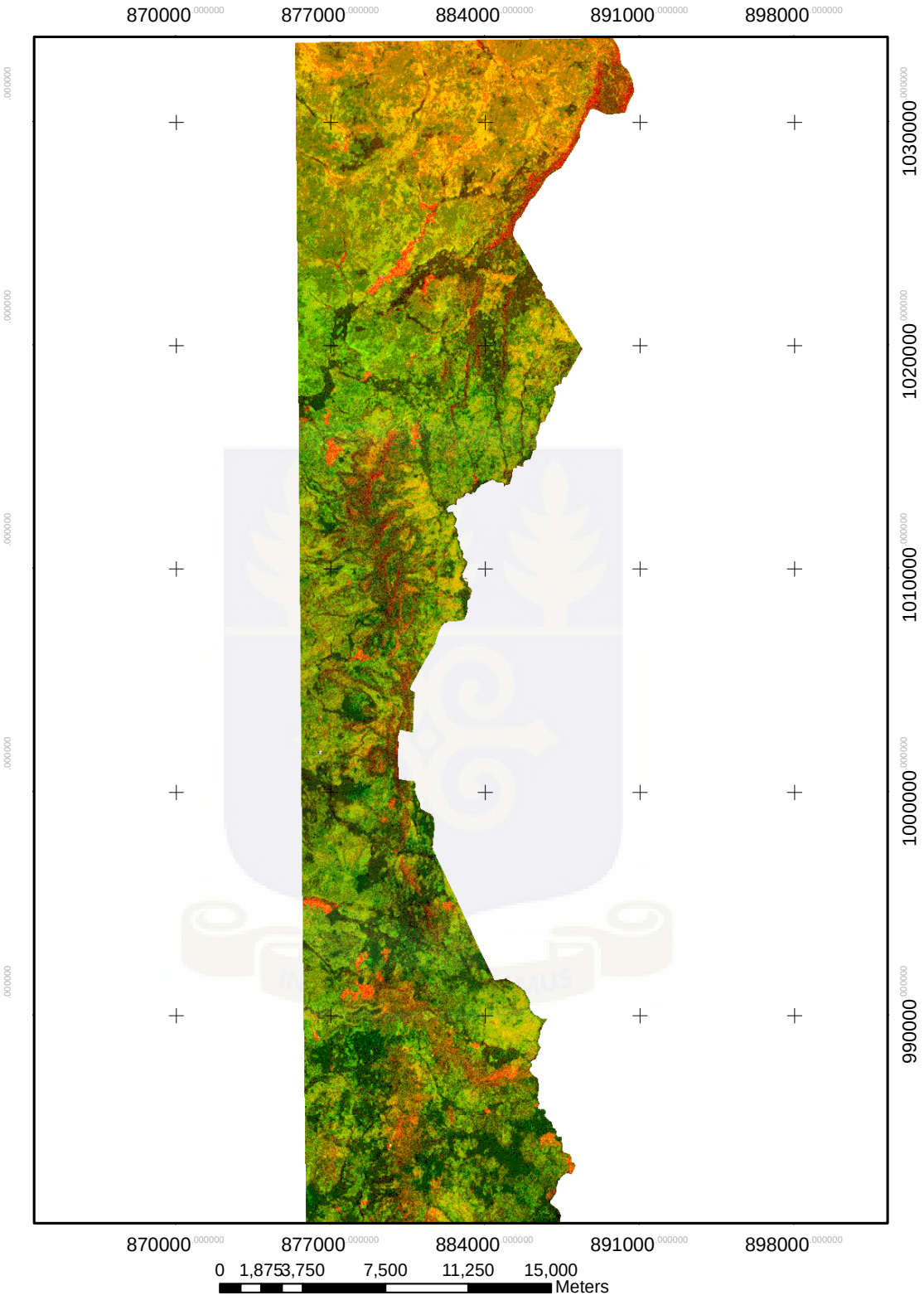

Figure 31: Chlorite mapping using ASTER band ratios R (9/4), R (7/5), and R (7/6), as RGB, respectively.

The red color represents chlorite occurrence in the study area (Fig. 31) utilizing the ratios code 9, 0, and 0 (RGB), for band ratios R (9/4), G (7/5), and B (7/6), respectively. Generally there is a close relation between chlorite anomalies and iron formations. It is dominant in the Sheini north license and are likely to be related to BIFs (locally, the BIF is cross-cut by numerous thin veinlets of quartz, amorphous silica, secondary hematite, chlorite (chamosite) and siderite. There is also a close correlation between chlorite anomalies and drainage indicating that much of the chlorite alteration is related to alluvium along river or stream valleys. It can be observed from figure 31 that, Chlorite anomalies are developed on the low lying terrain to the east and west of the iron formations and are mostly associated alluvium.

4.5. Comparison between the applied image enhancement methods

Multispectral data sets (LANDSAT ETM and ASTER) have been processed using three enhancement techniques, each with its advantages and disadvantages. Below are the comparisons among the three methods.

4.5.1. Color composite

In general, the correlation coefficient matrix plot simplifies the complex and tedious process of selecting three appropriate bands to be combined in color composite images. Although this method narrows the possible band combinations, its disadvantages include:

(a) Non uniformity of images due to assignment of colors based on the analyst consent.

(c) The method is scene dependent in that different correlation coefficient matrix plot are obtained for different image subsets

4.5.2. Principal component analysis (PCA)

This technique utilizes the generalized reflectance curve of the component of interest, such as hydrothermal alteration in which band ratios are considered in the choice of the best Principal Component, based on the ratio of their respective eigenvector values. For instance, to determine which PC best represent iron-bearing minerals depends on the eigenvector values of bands 3 and 1 in a LANDSAT ETM dataset. Likewise, the clay minerals are controlled by the eigenvector values of bands 5 and 7 reference to their generalized reflectance spectra curve of the USGS Library of minerals. The signs (+/-) of the eigenvector value loadings are considered in the ratioing process, because they determine which component of interest (Fe oxide or clay) would be represented as bright or dark pixels in the image. In selecting the optimum principal component, the two loadings should always be different in signs. Consequently, when the numerator is positive implies bright pixels, whereas when it is negative implies dark pixels will represent the feature of interest. Although this technique helps in identifying iron and clay minerals, it is not definitive in discriminating or naming the various possible minerals which may constitute the brighter color exhibited by a particular group of pixels at a specific location on the image.

4.5.3. Band ratioing (BR) method

Band ratioing involves division of reflection and absorption peaks and troughs of relevant bands resulting in an improvement of images regardless of illumination positions or terrain. Despite the improvement in image contrast by band ratioing, its weakness is demonstrated by the reduction in the reflection intensity of objects on the images. Also, there could be more than one mineral candidate for the same band ratio (e.g., the LANDSAT ETM ratio R (3/1) and R (5/7) are

generally used to discriminate iron- and clay-bearing minerals, respectively. That is ambiguous due to the presence of many iron and clay minerals within each category. The remedy to this method is by the application of ratio codes which specifically define which mineral is being mapped by each code. In brightness and ratio codes technique, the mineral library spectra is divided into deciles, with each decile of a spectral band or ratio is labeled from 9 for the highest decile, down to 0 for the lowest decile. A triplet combination of any three codes of 9, 0, 0 may be displayed in the primary colors of red, green, and blue (RGB), respectively, thus makes the mineral of interest to appear as red in the resulting image (Perry & Vincent, 2009).

The utilization of brightness and ratio codes (Vincent, 1997) facilitated identification of hydrothermal alteration minerals with greater ease than it would be with the other enhancement methods, which identify alteration zones generally, but not specifically in terms of particular diagnostic minerals or hydrothermal alteration indicators. Consequently, band ratioing is the best of all the methods applied in this research work.

CHAPTER FIVE

INTERPRETATION

5.1 Interpretation.

The satellite imagery was interpreted using ArcView GIS. The interpretation of the study area was generally undertaken at 1:25,000-1:30,000 scale. Reference was made to the geological map of the area that have been provided for each of the image data sets. A first pass interpretation was extracted by PC 3 on ETM band1, band3, band4 and band7 (Fig. 32) and PC6 on ASTER VNIR+SWIR (Fig. 33). Additional features were added using the other Landsat ETM+ and ASTER band combination as well as the black and white Landsat and ASTER images.

The alteration anomalies were defined by thresholding the alteration image on the basis of image statistics (two standard deviations) and asperities in the reflectance histograms for each of the alteration anomaly images. The validity of the applied remote sensing techniques can be determined by comparison between the applied methods and effectiveness of their results with spectral and non-spectral ground data (ground truth) in the exploration area. In the present study, there were no ground spectral data, and the validation was performed on a geological. A series of potential alteration images, for each of the mineral types selected, were produced and combined with a local geological map of the study area. The following maps produced would serve as guidance for further exploration in the study area due to the presence of ASTER and Landsat ETM+ derived alteration anomalies

Anomaly alteration information was divided into three levels by the multiple of standard deviation of principal component image.

5. 1.1. Iron-oxide anomaly alteration extraction

Iron-oxide anomaly alteration can be extracted by PC 3 on TM band1, band3, band4 and band7.

The final iron-oxide anomaly alteration distribution is presented in Figure 32.

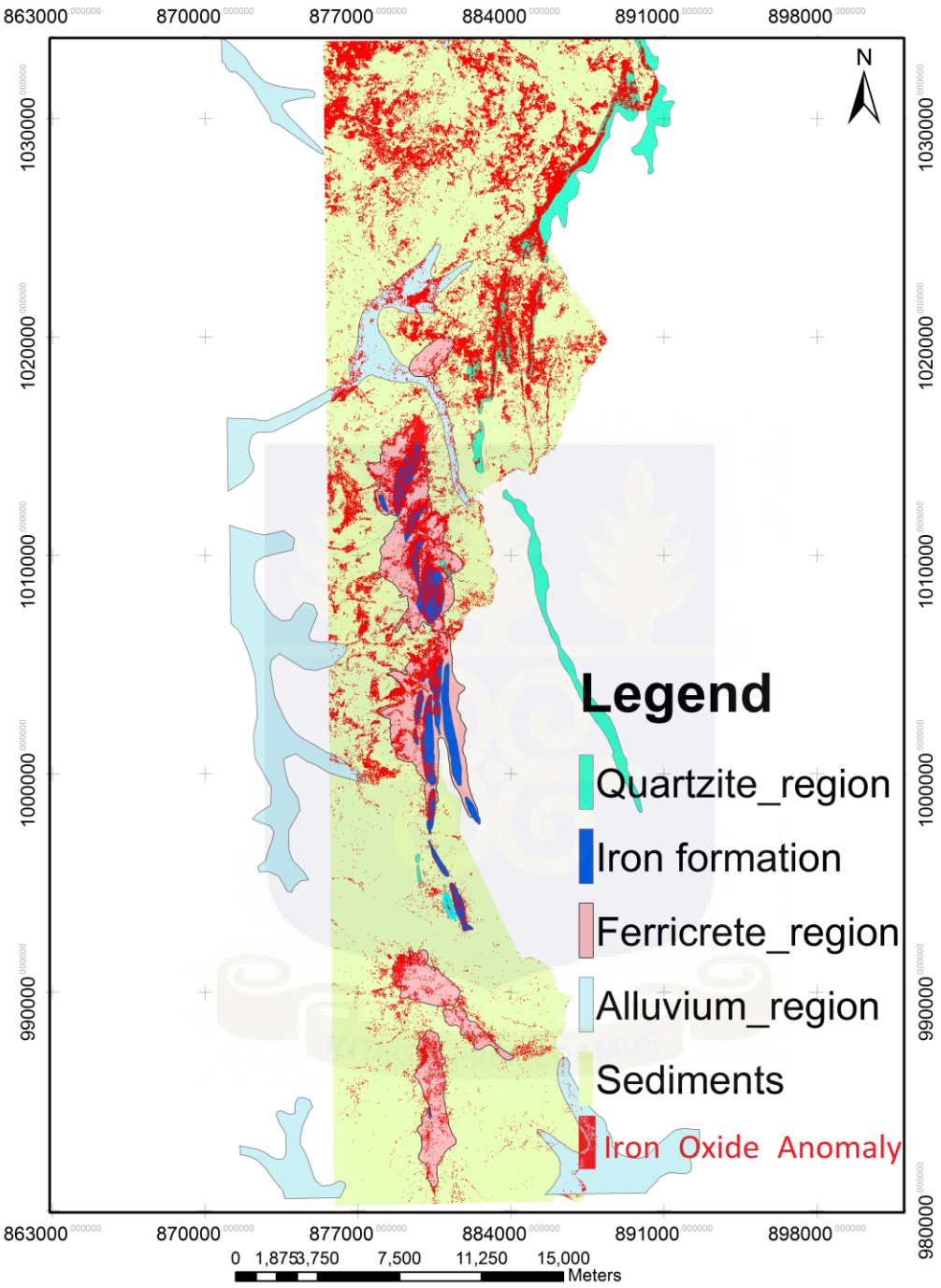

Figure 32: Final Iron oxide potential map for Sheini Hills

Iron oxide anomalies are associated with mapped quartzite in the northeast corner of the licence area which confirms the geology suggesting that the northern part of the study area is predominantly made up of Banded Iron Formations comprising interbedding between hematite and quartzite. It can also be observed that the iron oxide (haematite) anomalies occurs on the flanks of quartzite ridges in northeast of Sheini North license. According to figure 32, iron oxide anomalies is associated with the prominent mapped quartzite in the northeast corner of the license area .Iron oxides anomalies are also common across the license area to the west of the quartzite ridges. They correspond to rusty brown areas on the Landsat ETM 3-2-1 true color composite and appear to be related to bare cultivated soils on the ASTER 8-3N-1 image.

Although the Iron oxide anomalies within the central part of the Sheini License are generally small there is a good correlation between the main clusters of anomalies and the iron formations and ferricretes. It can be observed from figure 32 that the iron oxides (Haematite) anomalies are associated with ferricrete on flanks of the iron formation in the central part of the Sheini License Iron oxides anomalies are also developed in the central part of the Sheini South Licence. A cluster of anomalies occurs in the west-center. Another broad cluster is associated with ferricrete in the center of the licence area and are also common across the ferricrete in the south-center.

5. 1.2. Al-oh anomaly alteration extraction

The broad AL-OH anomaly alteration zone which is characterized by illite/muscovite (sericite) can be extracted by PC6 on ASTER VNIR+SWIR. The final Al-OH anomaly alteration distribution is presented in Figure 33.

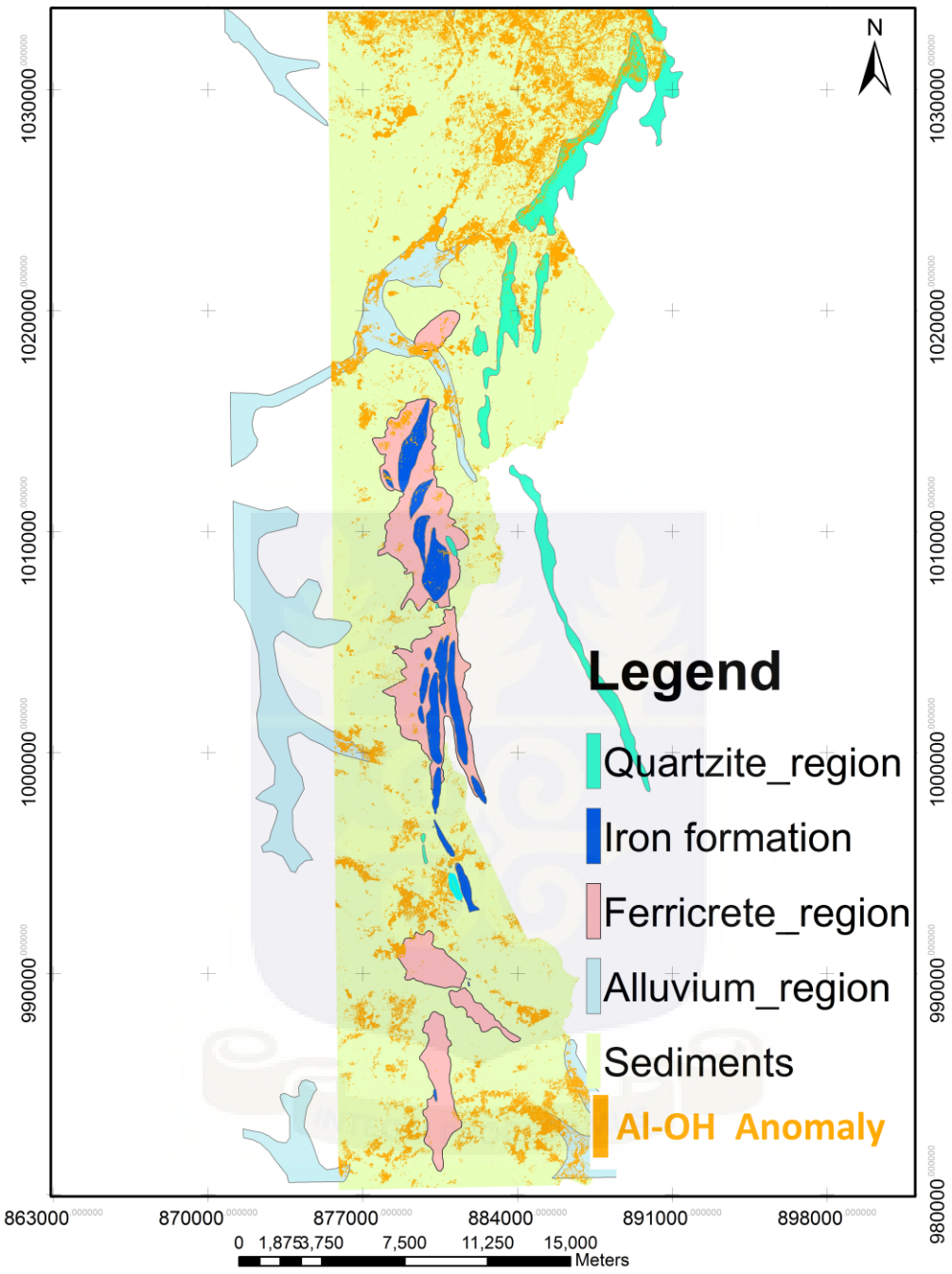

Figure 33: Final AL-OH potential map for Sheini Hills.

Generally there is a good correlation between the AL-OH alterations and the Voltaian Supergroup sediments which comprises mainly of flat lying greenish-grey to white sandstone, arkose, greywacke and mudstone. A cluster of clay anomalies are common across the licence area to the west of the quartzite ridges in the Sheini north licence. There is a good correlation between the iron oxide and clay mineral anomalies, although the iron oxide anomalies tend to be larger and commonly of higher intensity. A cluster of clay anomalies is located on the eastern flank of the BIFs in the north-center, they also related to drainages at the west-center and southwest of the Sheini licence. Several broad clay anomalies also occur at both the western and eastern parts of the Sheini south licence area.

CHAPTER SIX

CONCLUSIONS AND RECOMMENDATIONS

6.1 Conclusions

Multispectral remote sensing (LANDSAT ETM+ and ASTER) image enhancement and interpretation proved to be useful and resulted in multiple accomplishments.

- In the recognition, identification, detection, and delineation of hydrothermal alterations, and lithological rock units associated with iron ore deposits in the research area of the Sheini Hills, Ghana.

- The establishment of a template to identify hydrothermally altered areas from Landsat ETM and ASTER data

The selection of optimum 3-band color combination for hydrothermal alterations and lithological discrimination was performed by using the correlation matrix plot. The most informative band combination should include one visible, one NIR, and one SWIR. The method is best in selecting 3-band combination, but their assignment to the principal colors (RGB) solely depends on the selection by the analyst.

The use of ratio codes and spectral ratio techniques (Vincent, 1997) also enabled hydrothermal alteration and lithologic mapping based on diagnostic spectral signatures of iron and hydroxyl minerals. Generally, the LANDSAT band ratios R (5/7), R (3/1) and R (5.4), were utilized for mapping ferric, ferrous, and clay minerals, respectively.

The application of Feature Oriented Principal Component Selection (FPCS), which is based on the Crosta Technique of the Principal Component Analysis (PCA), was effective in identifying hydrothermal alteration zones in the area. To facilitate and reduce exploration expenses, it is best utilizing remote sensing capabilities for such tasks in order to obtain better coverage and accuracy with significantly reduced time and cost.

6.2 Recommendations

The application of remote sensing for mapping hydrothermal alteration zones association with iron ore in the Sheini area has been successful. Consequently, the technology is worth applying in the other part of the country that is characterized by highly favorable atmospheric conditions of arid terrain, which provide clear bedrock exposure. Integration of other exploration methods, such as geochemistry and geophysics, will improve the results of the present exploration approach.

As a follow up, field based structural analysis should be undertaken to verify and further develop the structural models that are associated with such deposits. Field analysis should also be conducted to define the stratigraphy and extent of thickening of the iron formations. The morphology and distribution of anomaly alteration in the study area can be used as important ore prospecting indicators in future geological investigation work. Further research in this respect coupled with ground truth at this study area, as well as in the other parts of the country will lead to better understanding of the conceptual model of mineralization, especially the association of alteration minerals with iron ore in the region known for such deposits.

REFERENCES

Abdelsalam, M.G., Stern, R.J., 1993. Tectonic evolution of the Nakasib suture, Red Sea Hills, Sudan. Evidence for a late Precambrian Wilson cycle. Journal of the Geological Society of London 150, 393–404.

Abdelsalam,M.G., Stern, R.J., 1996. Sutures and Shear Zones in the Arabian-Nubian Shield. Journal of African Earth Sciences 23, 289–310

Bekker, A., Slack, J.F., Planavsky, N., Krapez, B., Hofman, A., Konhauser, K.O., Rouxel, O.J.,2012. The Sedimentary Product of a Complex Interplay among Mantle, Tectonic, Oceanic, and Biospheric Processes, Economic Geology, v. 105, pp. 467-508.

Bobrov, S., Pentelkov, V., 1964. Report on the Geology and Minerals of the Eastern Part of the Bimbila-Zabzugu Area ,Archive Report No. 59, GSD, Accra, p. 1-55

Carlos A. Torres., Mineral Exploration Using GIS and Processed Aster Images, Advance GIS EES 6513 (Spring 2007).University of Texas at San Antonio

Carney, J.N., Jordan, C.J., Thomas, C.W., Condon, D.J., Kemp, S.J., and Duodo, J.A., 2010. Lithostratigraphy, sedimentation and evolution of the Volta Basin in Ghana. 183 (4), pp. 701-724.

Chavez PS, Berlin GL, Sowers LB 1982. Statistical method for selecting Landsat MSS ratios. J Appl Photogr Eng 8:23–30

Clark, R.N., Swayze, G.A., Gallagher, A., King, T.V.V., Calvin, W.M., 1993b. The US Geological Survey, Digital Spectral Library, Version 1, US Geological Survey Open File Report 93-592, 1340 p. <http://speclab.cr.usgs.gov> (August 1999).

Crosta, A. P., and Rabelo, A., 1993. Assessing of Landsat TM for hydrothermal alteration mapping in central western Brazil. Proceedings of Ninth Thematic conference geologic remote sensing Pasadinea, p. 1053-61, California, USA.

Crowley, J.K., Brickey, D.W., Rowan, L.C., 1989. Airborne imaging spectrometer data of the Ruby Mountains, Montana: mineral discrimination using relative absorption band depth images. Remote Sensing of Environment 29 (2), 121– 134.

Henderson, K.J, 2012. Technical report on Sheini Hills Iron Project, Ghana, Africa. Cardero Resource Corp. Unpublished report, p. 106 .

Hunt G.R., and Ashley R.P. Spectra of altered rocks in the visible and near infrared, Econ. Geol., 74(7): 1613–1629 (1979).

Jensen, J.R., 2005. Introductory Digital Image Processing. Person Prentice Hall, Upper Saddle River, p. 307 and 444.

Jacques, E. H., 1958, Report on the Sheini Iron Ore Deposits, Archive Report No. 85, GSD,Accra, p.1-47.

Knepper, D.H., Jr., 1989. Mapping hydrothermal alteration with Landsat Thematic Mapper data, in Lee, Keenan, ed., Remote sensing in exploration geology. A combined short course and field trip, 28th International Geological Congress Guidebook T182, p. 13–21.

Kröner, A., and Stern, R.J., 2004. Africa/Pan-African Orogeny. Encyclopedia of Geology, vol.1, Elsevier, Amsterdam.

Loughlin, W.P., 1991. Principal component analysis for alteration mapping. Photogrammetric Engineering and Remote Sensing 57, 1163-1169.

Ninomiya, Y., 2003a. A stabilized vegetation index and several mineralogic indices defined for ASTER VNIR and SWIR data. In Proceedings of the IEEE 2003 International Geoscience and Remote Sensing Symposium (IGARSS'03),vol.3, Toulouse, France, 21–25 July 2003, pp. 1552–1554.

Ninomiya, Y., 2003b. Advanced remote lithologic mapping in ophiolite zone with ASTER multispectral thermal infrared data. In: Proceedings of the IEEE 2003 International Geoscience and Remote Sensing Symposium (IGARSS'03), vol. 3, Toulouse, France, 21–25 July 2003, pp. 1561–1563

Osae, S.,Asiedu,D.K.,Banoeng-Yakubu, B., Koeberl, C., and Dampare, S.B., 2006.

Provenance and tectonic setting of Late Proterozoic Buem sandstones of southeastern Ghana: Evidence from geochemistry and derital modes. Journal of African Earth Sciences.44, pp. 85-96.

Perry, J., and Vincent, R. K., 2009. ASTER Brightness and Ratio Codes for Minerals: Application to Lithologic Mapping in the West-Central Power River Basin, Wyoming. Reviews in Economic Geology, v. 16, p. 143-168.

Perry, J., 2003, An investigation into the use of ASTER (Advance Space-borne Thermal Emission and Reflection Radiometer) data for geologic mapping in the Powder River basin, Wyoming: Unpublished MS thesis, Bowling Green, Ohio, Bowling Green State University, 121p.

Pour, B.A., Hashim, M., Marghany, M., 2011. Using spectral mapping techniques on short wave infrared bands of ASTER remote sensing data for alteration mineral mapping in SE Iran. International Journal of the Physical Sciences 6 (4), 917–929.

Rowan LC, Mars JC (2003) Lithologic mapping in the Mountain Pass,California area using Advanced Spaceborne Thermal Emission and Reflection Radiometer (ASTER) data. Remote Sens Environ 84:350–366

Rockwell, B.W., Hofstra, A.H., 2008. Identification of quartz and carbonate minerals across northern Nevada using ASTER thermal infrared emissivity data Implications for

geologic mapping and mineral resource investigations in well-studied and frontier areas. Geosphere 4 (1), 218–246.

Sabins, F.F., 1997. Remote Sensing, Principles and Interpretation, 3 ed, Freeman, New York.

Salem SM, Arafa SA, Ramadan TM, El Gammal ESA (2011) Exploration of copper deposits in Wadi El Regeita area, Southern Sinai, Egypt, with contribution of remote sensing and geophysical data. Arabian Journal of Geosciences.

Vincent, R. K., and F. J. Thomson, 1972. Rock-Type Discrimination from Rationed Infrared Scanner Images of Pisgah Crater, California, Science, Vol. 175, pp. 986-988.

Vincent, R. K. 1997. Fundamentals of Geological and Environmental Remote Sensing. Prentice Hall, 370p.

Washington, D.C.Drury, S.A. (1987). Image Interpretation in Geology. Chapman and Hall, London, 283 p.

Wright, J.B. Hastings, D.A., Jones, W.B., Williams, H.R., 1985. Geology and Mineral Resources of West Africa. George Allen and Unvin, London, pp. 56-82.

Yamaguchi, Y.I., Fujisada, H., Kudoh, M., Kawakami, T., Tsu, H., Kahle, A.B., Pniel,

M., 1999. ASTER instrument characterization and operation scnorio. Advanced Space Research 23 (8), 1415–1424.